

2015

Examining spectral variations in localized lunar dark mantle deposits

Erica R. Jawin

European Space Research and Technology Center, Noordwijk, Netherlands, Erica_Jawin@brown.edu

Sebastien Besse

European Space Research and Technology Center, Noordwijk, Netherlands

Lisa R. Gaddis

USGS Astrogeology Science Center, Flagstaff, Arizona

Jessica M. Sunshine

University of Maryland

James W. Head

Brown University

See next page for additional authors

Follow this and additional works at: <http://digitalcommons.unl.edu/usgsstaffpub>

Jawin, Erica R.; Besse, Sebastien; Gaddis, Lisa R.; Sunshine, Jessica M.; Head, James W.; and Mazrouei, Sara, "Examining spectral variations in localized lunar dark mantle deposits" (2015). *USGS Staff -- Published Research*. 861.
<http://digitalcommons.unl.edu/usgsstaffpub/861>

This Article is brought to you for free and open access by the US Geological Survey at DigitalCommons@University of Nebraska - Lincoln. It has been accepted for inclusion in USGS Staff -- Published Research by an authorized administrator of DigitalCommons@University of Nebraska - Lincoln.

Authors

Erica R. Jawin, Sebastien Besse, Lisa R. Gaddis, Jessica M. Sunshine, James W. Head, and Sara Mazrouei

RESEARCH ARTICLE

10.1002/2014JE004759

Key Points:

- Spectra were analyzed of three localized pyroclastic dark mantle deposits
- Glass-bearing materials were identified in all DMDs
- Two new localized DMDs were identified in Dryden T and S craters

Correspondence to:

E. R. Jawin,
Erica_Jawin@brown.edu

Citation:

Jawin, E. R., S. Besse, L. R. Gaddis, J. M. Sunshine, J. W. Head, and S. Mazrouei (2015), Examining spectral variations in localized lunar dark mantle deposits, *J. Geophys. Res. Planets*, 120, 1310–1331, doi:10.1002/2014JE004759.

Received 13 NOV 2014

Accepted 21 JUN 2015

Accepted article online 24 JUN 2015

Published online 29 JUL 2015

Examining spectral variations in localized lunar dark mantle deposits

Erica R. Jawin^{1,2,3}, Sebastien Besse¹, Lisa R. Gaddis⁴, Jessica M. Sunshine⁵, James W. Head³, and Sara Mazrouei^{1,6}

¹European Space Research and Technology Center, Noordwijk, Netherlands, ²Department of Astronomy, Mount Holyoke College, South Hadley, Massachusetts, USA, ³Department of Earth, Environmental, and Planetary Sciences, Brown University, Providence, Rhode Island, USA, ⁴USGS Astrogeology Science Center, Flagstaff, Arizona, USA, ⁵Department of Astronomy, University of Maryland, College Park, Maryland, USA, ⁶Now at Department of Earth Sciences, University of Toronto, Ontario, Canada

Abstract The localized lunar dark mantle deposits (DMDs) in Alphonsus, J. Herschel, and Oppenheimer craters were analyzed using visible-near-infrared spectroscopy data from the Moon Mineralogy Mapper. Spectra of these localized DMDs were analyzed for compositional and mineralogical variations within the deposits and were compared with nearby mare basalt units. Spectra of the three localized DMDs exhibited mafic absorption features indicating iron-rich compositions, although the DMDs were spectrally distinct from nearby mare basalts. All of the DMDs contained spectral signatures of glassy materials, suggesting the presence of volcanic glass in varying concentrations across the individual deposits. In addition, the albedo and spectral signatures were variable within the Alphonsus and Oppenheimer crater DMDs, suggesting variable deposit thickness and/or variations in the amount of mixing with the local substrate. Two previously unidentified localized DMDs were discovered to the northeast of Oppenheimer crater. The identification of high concentrations of volcanic glass in multiple localized DMDs in different locations suggests that the distribution of volcanic glass across the lunar surface is much more widespread than has been previously documented. The presence of volcanic glass implies an explosive, vulcanian eruption style for localized DMDs, as this allows volcanic glass to rapidly quench, inhibiting crystallization, compared to the larger hawaiian-style eruptions typical of regional DMD emplacement where black beads indicate a higher degree of crystallization. Improved understanding of the local and global distributions of volcanic glass in lunar DMDs will further constrain lunar degassing and compositional evolution throughout lunar volcanic history.

1. Introduction

Deposits of lunar pyroclastic material, referred to as dark mantle deposits (DMDs), have been studied and mapped since the Apollo era [Wilhelms, 1968; Wilhelms and McCauley, 1971; Head, 1974; Gaddis et al., 1985, 2003; Weitz et al., 1998; Gustafson et al., 2012]. These fine-grained, low-albedo deposits are understood to be volcanic in nature [Wilson and Head, 1981]. They are characterized by unique spectral signatures [Pieters et al., 1973] and low radar returns [Gaddis et al., 1985] owing to large amounts of Fe-bearing volcanic glass and a paucity of scattering surfaces >50 cm. Morphologically, these deposits appear to mantle underlying material, smoothing and subduing small-scale topographic features [Head, 1974].

Previous studies have identified over 100 DMDs across the lunar surface (Figure 1), ranging in areal extent from <10 km² to ~50,000 km² [Gaddis et al., 2003; Gustafson et al., 2012]. The largest of these (>1000 km²) are known as “regional” DMDs, while the smaller (typically ~200–500 km²) are termed “localized” DMDs [Gaddis et al., 1985]. Localized DMDs, such as those in Alphonsus crater (Figure 2), often consist of multiple local patches, which in this work are referred to as subdeposits. Additionally, regional DMDs are generally located near mare-filled basins and superimposed on highlands materials, while localized DMDs are often associated with fissures in large, Imbrian to pre-Imbrian aged floor-fractured craters [Head, 1974; Schultz, 1976; Weitz et al., 1998; Jozwiak et al., 2012]. Emplacement style is believed to vary between these two types of DMDs. Regional DMDs are understood to be the result of hawaiian-style eruptions, characterized by long-duration fire-fountaining events [Wilson and Head, 1981], while smaller, localized DMDs are inferred to have formed from sporadic, explosive vulcanian-style eruptions [Head and Wilson, 1979; Hawke et al., 1989].

This document is a U.S. government work and is not subject to copyright in the United States.

©2015. American Geophysical Union.
All Rights Reserved.

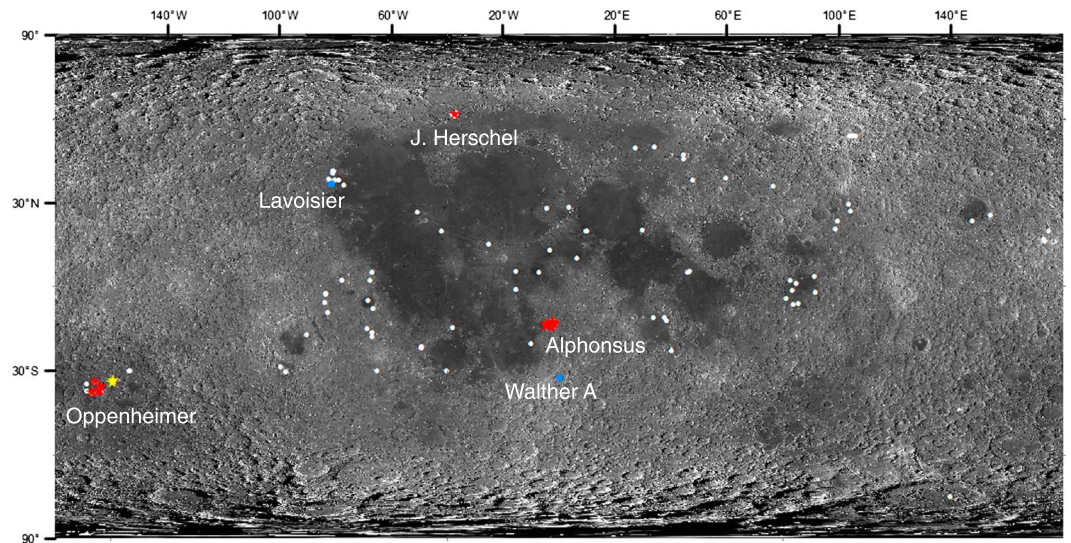


Figure 1. Global distribution of DMDs (white circles) [Gaddis et al., 2003; Gustafson et al., 2012] on a Wide Angle Camera global mosaic. Red stars indicate the location of localized DMDs studied here; yellow stars indicate the location of new localized DMDs identified in this work. Blue dots indicate the location of localized DMDs in Lavoisier and Walther A craters analyzed previously by Souchon et al. [2013] and Besse et al. [2014], respectively.

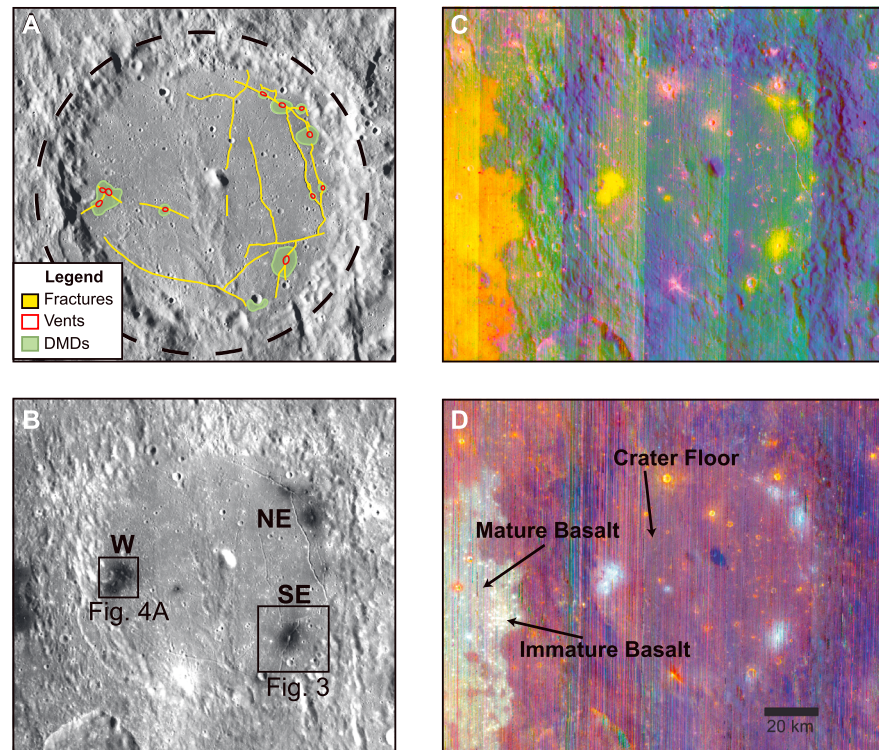


Figure 2. Alphonsus crater. (a) Sketch map with a Kaguya TC evening mosaic as the basemap. (b) M^3 1 μm albedo map. DMDs appear dark, and specific subdeposits studied here are labeled (see Table 2 for details on each subunit). (c) RGB color composite image using R: IBD 1000 nm, G: BD 1900 nm, and B: R 1580 nm. (d) RGB color composite image using R: BD 950 nm, G: BD 1050 nm, and B: BD 1250 nm. Spectra of mare basalts and crater floor used in Figure 4d are identified here. Vertical banding in Figure 2c is a residual from the photometric correction [Besse et al., 2013].

Collectively, DMDs are believed to represent the eruption of gas-rich magmas from dikes originating from deep within the Moon (>300 km depths), bringing to the surface a key suite of mafic minerals which crystallized from primitive, unfractionated magmas [Delano and Livi, 1981]. Compositional and mineralogical analyses from remote sensing observations and laboratory measurements [Pieters et al., 1973; Adams et al., 1974; Gaddis et al., 1985, 2000, 2003; Hawke et al., 1989; Weitz et al., 1998] have found that DMDs are composed of mafic minerals enriched in iron and titanium with volatile-rich coatings. Many regional DMDs were found to contain large amounts of Fe²⁺-bearing volcanic glass beads, iron- and titanium-rich glass, and devitrified beads of similarly mafic composition [Pieters et al., 1973; Adams et al., 1974; Gaddis et al., 1985; Lucey et al., 1986; Weitz et al., 1998, 1999]. Iron-rich volcanic glass has also recently been clearly identified using remote sensing observations in localized DMDs [Besse et al., 2014; Horgan et al., 2014]. In addition, chromium-rich spinel has been identified in the Sinus Aestuum DMD [Sunshine et al., 2010, 2014; Yamamoto et al., 2013].

Early studies [Hawke et al., 1989] based on Earth-based telescopic data (1–5 km footprint) proposed three classes of localized DMDs whose major distinctions included the presence of mostly basaltic material, a combination of basalt and wall rock material, and a component of juvenile material including olivine and pyroxene. However, later studies [e.g., Gaddis et al., 2000] using Clementine multispectral data (100–200 m/pixel, 0.415–1.0 μm) did not identify an olivine component in any of the localized deposits studied, with the exception of J. Herschel crater. More recently, Besse et al. [2014] suggested that the olivine detection in previous studies could have been mistaken for volcanic glass mixed with pyroxene in data sets that only cover the 1 μm absorption and do not include the 2 μm region. This possibility was also raised by Horgan et al. [2014] in their analysis of ferrous mineral mixtures in the laboratory and of hyperspectral remote sensing data of the Moon and Mars.

While many studies have been made of lunar DMD mineralogy with remote sensing data, new data from the Moon Mineralogy Mapper (M³) aboard the Chandrayaan-1 spacecraft provide high spatial (~140 m/pix or ~280 m/pix) and spectral (0.4–3 μm) resolution data which now allow for more detailed characterization of DMD mineralogy. The M³ wavelength range allows for the analysis of both the 1 and 2 μm absorption bands, which include the spectral range necessary to distinguish between a variety of mafic minerals [Pieters et al., 2009; Green et al., 2011].

As DMD materials are volatile-enriched and less fractionated relative to mare basalts, they have been interpreted to represent remnant deposits of ancient volcanic eruptions on the Moon and provide clues to the nature of the early lunar interior [Heiken et al., 1974; Delano, 1986; Shearer and Papike, 1993; Papike et al., 1998; Shearer et al., 2006] and to the distribution of potential resource materials for future exploitation [Hawke et al., 1990; Duke et al., 2006]. Volcanic glasses are believed to be sourced from primary magmas that have not undergone significant crystal/liquid fractionation [Delano, 1986; Jones and Delano, 1989], although more recent studies have suggested primitive melts may not be required and volcanic glass parent magmas may have been sourced from interstitial melts and high-titanium late-stage cumulates [Elkins-Tanton et al., 2011]. These lunar glasses are therefore important in characterizing the lunar interior and represent a key stage in the origin and evolution of basaltic magmatism on the Moon. The nature of these deposits, including the characterization of the diversity of mineralogy within and between different deposits, must be explained in all models of the formation, ascent, and emplacement of lunar magmas. In addition, comparing the spectral variation between DMDs and mare basalts will lead to key insights into the volatile variation and compositional evolution during lunar basalt ascent and eruption [Weitz et al., 1998, 1999].

In this study, three localized DMDs were analyzed using spectral data from M³ in an effort to (a) document the mineralogy of these deposits, (b) characterize the amount of mineralogical variation within and between each deposit and between isolated areas of the same localized DMD, and (c) compare the mineralogy of each DMD to the nearest deposit of mare basalt. The goals of this work are to study the variations in deposit mineralogy and internal structure (i.e., crystalline or glassy materials) observed in lunar localized DMDs, to assess their genetic relationships to nearby mare deposits, and to better understand how factors such as mineralogy and internal structure vary within and among deposits that originate as both effusive and explosive volcanic eruptions on the Moon.

2. Background and Data Collection

2.1. Spectroscopic Background

The main rock-forming minerals on the Moon include plagioclase, pyroxenes, and olivine [Wood *et al.*, 1970]. Variations in elemental composition and crystal structure between these minerals distinguish them in near-infrared spectroscopy. Variations in the presence and concentration of magnesium, ferrous iron, and calcium, and their location within the crystal structure of mafic minerals control the position, depth, and shape of spectral absorption bands due to energy transfers within the crystal lattice [Burns, 1993]. Additional contributions to variations in these energy transfers include site occupancy in the M1 and M2 crystallographic sites and the inclusion of additional cations in the crystal structure [Burns, 1970, 1993; Cloutis, 2002; Horgan *et al.*, 2014].

Pyroxenes are characterized by distinct absorption bands around 1 and 2 μm , with low-calcium pyroxenes displaying bands shifted to slightly shorter wavelengths, and high-calcium pyroxenes exhibiting bands at slightly longer wavelengths with increasing Ca and Fe [Cloutis and Gaffey, 1991; Klima *et al.*, 2011]. Olivine, however, has a complex absorption centered near 1 μm , with no absorption at 2 μm . Therefore, olivine-rich lunar deposits are characterized by a broad 1 μm absorption band which is enhanced relative to the 2 μm band. Spinel has also been identified at the Sinus Aestuum DMD [Sunshine *et al.*, 2010, 2014; Yamamoto *et al.*, 2013] on the basis of its strong 2 μm band and absence of a 1 μm band [Cloutis *et al.*, 2004].

While composition and mineralogy are the dominant control of spectral signatures, several other factors will also affect the behavior of reflectance spectra in the visible to near-infrared wavelengths (VIS-NIR), including grain size, degree of space weathering, and internal structure (i.e., crystallinity). Grain size has a direct control on absorption band strength, as small grain sizes are characterized by surficial or first-surface scattering; materials with larger grain size, by comparison, have a higher degree of internal reflection and absorption, leading to deeper absorption bands [e.g., Hapke, 1981]. Space weathering also greatly affects absorption band depth and spectral slope, in particular on lunar targets. Spectra of space-weathered surfaces demonstrate red-sloped continua and weaker absorption bands than freshly exposed surfaces, due to the accumulation of fine-grained nanophase iron (npFe⁰) [Morris, 1976; Pieters *et al.*, 1993; Noble *et al.*, 2007].

The crystallinity of a surface also controls absorption band position and depth. For example, amorphous material rich in transition metals, such as Fe-bearing volcanic glass (e.g., Apollo 17 orange glass, as well as the Apollo 17 black beads), is known to exhibit broad, shallow absorption bands [Adams and McCord, 1971; Bell *et al.*, 1976]. Spectra of these volcanic glasses show 1 and 2 μm bands, which are shifted to slightly longer and shorter wavelengths, respectively, compared to pyroxenes, making them distinguishable from other mafic minerals. These volcanic glass characteristics were recently observed in lunar DMDs from orbit [Besse *et al.*, 2014; Horgan *et al.*, 2014], implicating an explosive volcanic origin for these deposits [Weitz *et al.*, 1998, 1999].

2.2. Moon Mineralogy Mapper Observations

In this analysis, Level 2 v1.0 data released to the Planetary Data System (PDS) [Malaret *et al.*, 2011] are used. Level 2 calibrated data include geometric and radiometric [Boardman *et al.*, 2011; Green *et al.*, 2011], thermal [Clark *et al.*, 2011], and photometric [Besse *et al.*, 2013] corrections. Additional ground truth corrections developed to address subtle shape anomalies seen in weak absorptions of spectra from feldspathic terrains [Isaacson *et al.*, 2013] are not applied to this work, as spectra of the DMDs reported here include relatively strong absorptions from mafic deposits. Finally, empirical cross-track corrections to remove image-to-image boundaries, described by Besse *et al.* [2013], are applied to each individual mosaic and listed in Table 1.

A continuum removal was applied to the spectra to highlight the position and shape of the 1 and 2 μm bands. The continuum is approximated by a straight line fit between 0.73 and 1.62 μm and 1.62 and 2.58 μm for the 1 and 2 μm bands, respectively (see vertical lines in Figure 4a) [Besse *et al.*, 2014]. The same continuum removal was applied to all spectra in this work. It is important to note that defining the continuum with this function may have an adverse effect on spectra with certain mineralogies containing low 2 μm band centers (for example, low-calcium pyroxenes or orthopyroxenes) or low interband peaks (typical of many pyroxenes with minimal plagioclase content) or spectra with nonlinear slopes.

In order to permit comparisons of the spectral signatures of the various DMDs, it is important to minimize the effect of detector temperature variations that are inherent in the M³ data set (see Isaacson *et al.* [2013] for a

Table 1. Summary of Images Properties Used for Each Target Mosaic^a

Target	Image Used	Average Phase Angle (Degrees)	Optical Period	Average Resolution (m/pix)	Cross-track Correction	Centered Latitude/Longitude
Alphonsus	M3G20090205T171614_V01_L2	49.4	OP1B	140	PDS	−13.33/−3.37
	M3G20090205T193313_V01_L2					
	M3G20090205T211213_V01_L2					
	M3G20090205T233034_V01_L2					
	M3G20090206T010833_V01_L2					
	M3G20090206T030351_V01_L2					
Herschel	M3G20090208T080838_V01_L2	66.3	OP1B	140	PDS	61.5/−41.1
	M3G20090208T100012_V01_L2					
	M3G20090208T114652_V01_L2					
	M3G20090208T135610_V01_L2					
	M3G20090208T160125_V01_L2					
	M3G20090208T175211_V01_L2					
	M3G20090208T194335_V01_L2					
	M3G20090208T214811_V01_L2					
	M3G20090208T233940_V01_L2					
	M3G20090209T014431_V01_L2					
	M3G20090209T033051_V01_L2					
	M3G20090209T054031_V01_L2					
	M3G20090209T072710_V01_L2					
	Oppenheimer					
M3G20090620T181042_V01_L2						
M3G20090621T022743_V01_L2						
M3G20090621T065503_V01_L2						
M3G20090621T193712_V01_L2						

^aThe center coordinates of the M³ mosaic, as well as relevant spatial information, are given for each localized DMD target. The available optical period coverage for each region is as follows: Alphonsus was completely covered by OP1B, J. Herschel was partially covered by OP2A and completely covered by OP1B, and Oppenheimer was partially covered by OP2C.

description of temperature variations within the various M³ optical periods (OP1A, OP1B, OP2A, OP2B, and OP2C). Spectral analyses of the DMDs analyzed in this study were limited to optical periods OP1B and OP2C. This was done in an attempt to minimize the variations in absolute reflectance between DMDs, although M³ data in different optical periods exist for the DMDs analyzed in this study (details about the optical periods used are listed in Table 1). The specific optical periods were chosen as they provided the most uniform coverage over the chosen study areas as well as the most optimal viewing conditions based on the available data. The observations for the DMDs in Alphonsus and J. Herschel craters were taken during the optical period OP1B and provide both the highest spatial resolution and the coldest detector temperatures, while observations of Oppenheimer crater were taken during the optical period OP2C, when the spacecraft was observing from a higher altitude (and thus lower spatial resolution) and at higher detector temperatures. Because of the combination of data from different optical periods, the comparisons of the DMDs (see section 4) include the band shape, position, and relative band depth, but not absolute reflectance.

As mentioned above, absorption band shape and position can be used to determine deposit mineralogy. The relative strengths of the 1 and 2 μm absorption bands can also be useful in distinguishing mineralogical variation, as has been done in spectral analyses of asteroids [e.g., Gaffey *et al.*, 1993]. Using ratio values of absorption band depth is a valid method of analysis as ratios are independent of the absolute reflectance values. These are reported in terms of the 2/1 μm band depth ratio values and were calculated for key spectra (see Table 3 and the discussion in section 4), in addition to band center values for the 1 and 2 μm bands. These band center values were calculated by finding the minimum absorption depth for both the 1 and 2 μm bands and fitting a fourth-order polynomial within 80 nm of the minimum, with a fit resolution of 5 nm, in a similar manner to Horgan *et al.* [2014]. This polynomial provides a more accurate band minimum position than the M³ band spacing allows. Band center values were assumed to be the location of the band minimum. The band depth values are calculated by subtracting the relative reflectance value found at the band minimum from 1, in the continuum-removed spectra. This is a more rigorous approach than that of Besse *et al.* [2014], which estimated a band position based on a visual inspection of the spectra.

Table 2. Summary of DMD Properties^a

DMD	Subdeposits	Central Longitude	Central Latitude	Size (km ²)
Alphonsus	W	4.1°W	13.6°S	93
	SE	2°W	14.3°S	95
	NE	1.7°W	12.8°S	97
J. Herschel	Continuous	36.6°W	61.7°N	630
Oppenheimer	N	165.5°W	33.56°S	76
	E	163.2°W	35.3°S	26
	SE	163.4°W	37°S	190
	SSE	134.6°W	37.1°S	44
	S	166.9°W	37.9°S	890 ^b
Dryden S	Continuous	159°W	34.3°S	150
Dryden T	Continuous	159.2°W	33°S	245

^aProperties are listed for the subdeposits analyzed in this study; naming is continued throughout text and figures. Coordinates were mapped using a combination of Lunar Reconnaissance Orbiter Camera Wide Angle Camera global mosaic, M³ 1 μ m albedo map, and M³ RGB color composite image (R: IBD 1000 nm, G: BD 1900 nm, and B: R 1580 nm). Note that size values may differ slightly from the areas reported by *Gaddis et al.* [2003].

^bThis area is a lower estimate, as only a portion of the Oppenheimer S deposit was covered by M³ data.

To highlight the spectral properties of the DMDs in a regional context, color maps were created based on the spectral characteristics of mafic minerals. Products such as integrated band depth (IBD) can reveal details of the DMDs such as spinel-rich composition of the Sinus Aestuum deposits, variations in olivine content, and the nature of pyroxenes. IBD integrates the band depth over the entire spectral range of the 1 or 2 μ m band relative to a straight continuum, whereas band depth (BD) calculates the depth relative to the continuum at a given wavelength. Details about the IBDs and BDs are given in *Besse et al.* [2014] in the similar context of localized DMD analyses. Color maps in this work are created using RGB values of the IBD at 1000 nm, BD at 1900 nm, and reflectance at 1580 nm, respectively, as well as BD at 950 nm, BD at 1050 nm, and BD at 1250 nm (e.g., Figures 2b and 2c). The variations in absorption strengths at these three wavelengths determine the relative color on the map.

Because of the shallow absorptions observed in the DMDs, multiple pixels were averaged to obtain a higher signal-to-noise ratio (see colored outlines in Figures 4–6). Each spectral analysis area was drawn so that the maximum number of pixels was included, while excluding material from differing spectral units. Additionally, spectra have been smoothed with a moving average where each point is the average of itself and the two adjacent data points. The same smoothing technique is applied to all spectra.

The context images that support the spectroscopic products are mosaics derived from high-resolution images from the Kaguya (SELENE) Terrain Camera (TC) [*Haruyama et al.*, 2008], with shadows and topography emphasized by either morning or evening illumination. These mosaics, which are highly complementary to the high-sun multispectral views from M³, provide resolutions of 7–10 m/pix and are valuable in the identification of volcanic features such as vents, fractures, and rilles.

2.3. DMD Regions of Interest

The three localized DMDs occur in floor-fractured craters, including Alphonsus crater (3°W, 13.6°S, 110 km diameter), J. Herschel crater (36.6°W, 61.7°N, 154 km diameter), and Oppenheimer crater (166°W, 35.5°S, 201 km diameter) (Figure 1). These units were chosen because of their range of locations across the lunar surface, coverage in M³ data, and morphology: these deposits are either isolated individual dark subdeposits surrounding a noncircular vent (e.g., the southeast subdeposit in Alphonsus crater, Figure 2a and Table 2) or in some cases a combination of multiple subdeposits. In the latter case, each subdeposit surrounds one or more clustered vents, which are often associated with fractures (e.g., the west subdeposit in Alphonsus crater, Figure 2b and Table 2). The morphology of these localized DMDs allows for detailed spectral analyses of the pyroclastic material, as well as comparisons between pyroclastic material, crater floor material, and surrounding mare basalts.

In this work, M³ data are applied to identify mineralogical variations within and between the DMDs and to identify the presence of crystalline or amorphous (i.e., glassy) material. Where possible (dependent on deposit morphology, size, and resolution in the M³ data), radial analyses were obtained in order to observe

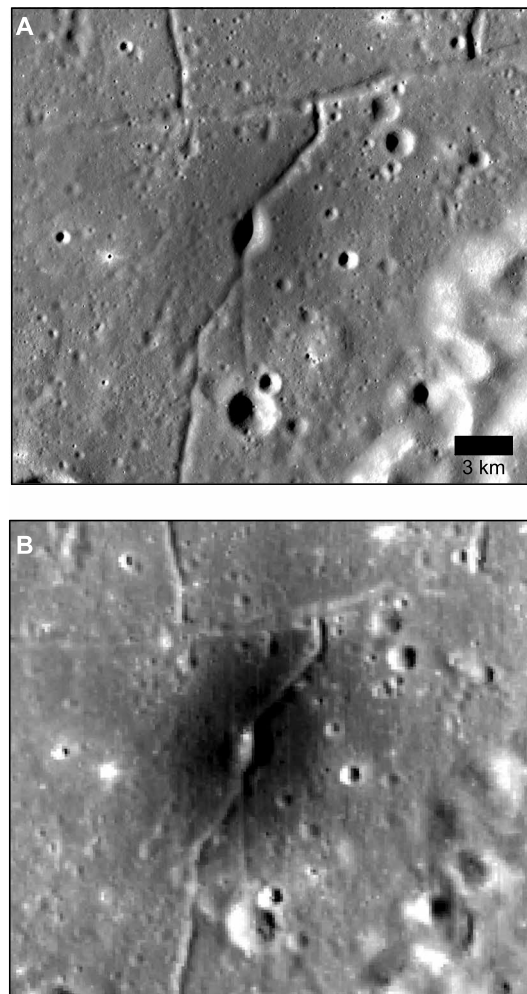


Figure 3. Alphonsois southeast subdeposit (a) Kaguya TC evening mosaic and (b) M^3 1 μm albedo map (see Figure 2b for context). Note the diffuse edges and variation in albedo across the deposit.

Based on M^3 albedo maps and color composite images, it is possible to identify several distinct subdeposits throughout Alphonsois crater (Figure 2). The largest of these deposits are located in the western, southeastern, and northeastern portion of Alphonsois crater, while smaller subdeposits are located west of the central peak, near the eastern rim of the crater, and near the southern rim of the crater (Figure 2a). Spectra were extracted from the largest of the Alphonsois DMD subdeposits, namely, those in the west, southeast, and northeast portion of the crater floor, as these provided the most areally expansive deposits of pyroclastic material in the crater, which allowed for a more detailed spectral analysis. While formal names exist for most of the vents in Alphonsois crater [after Head and Wilson, 1979], including those studied in this work, the subdeposits analyzed in this study will be referred to informally by their location within the crater as west, southeast, and northeast, as labeled in Figure 2b.

Color maps created using M^3 data highlight the DMDs and help to distinguish them from the surrounding materials (Figures 2c and 2d). The DMDs in these color schemes are easily distinguishable due to their absorption bands at both 1 and 2 μm relative to the weak absorption bands exhibited by the crater floor.

spectral variations based on location. In these DMDs, subdeposits were analyzed at regularly increasing distances from a volcanic vent. Additionally, M^3 data were used to assess whether there are detectable albedo variations that may suggest changes in mineralogy as distance from a vent increases. Finally, each localized DMD studied here is found in close proximity to a mare basalt unit; this proximity provides an opportunity to compare spectral signatures between explosive and effusive styles of volcanism and to assess the variation in mineralogy and composition between the two. This may aid in determining if the DMD and mare units were comagmatic. Spectral analyses from the DMDs in Alphonsois, J. Herschel, and Oppenheimer craters are compared to spectra of the DMDs located in Lavoisier and Walther A craters [Souchon et al., 2013; Besse et al., 2014]. These additional spectra from Lavoisier and Walther A provide other examples of analyses using high-resolution M^3 data of DMDs in floor-fractured craters, as well as a previously detected example of volcanic glass in the Walther A DMD [Besse et al., 2014].

3. Localized Dark Mantle Deposits

3.1. Alphonsois Crater

Alphonsois, a pre-Imbrian impact crater with a diameter of 110 km, is located in the lunar highlands east of Mare Nubium (Figure 1). The crater exhibits multiple floor fractures (Figure 2a), on which the individual DMDs are generally located. There are five main subdeposits on the floor of the crater, including 13 known vents and two “possible vents” still under investigation [Gaddis et al., 2011]. The volcanic vents are distinguishable from impact craters based on their irregular shape, subdued or absent crater rim, location inside DMD subdeposits, and frequent associations with fractures on the crater floor (Figures 2a and 3). The DMDs are easily identifiable by their low albedo in Kaguya TC images and M^3 albedo maps relative to the floor of Alphonsois crater (Figure 3).

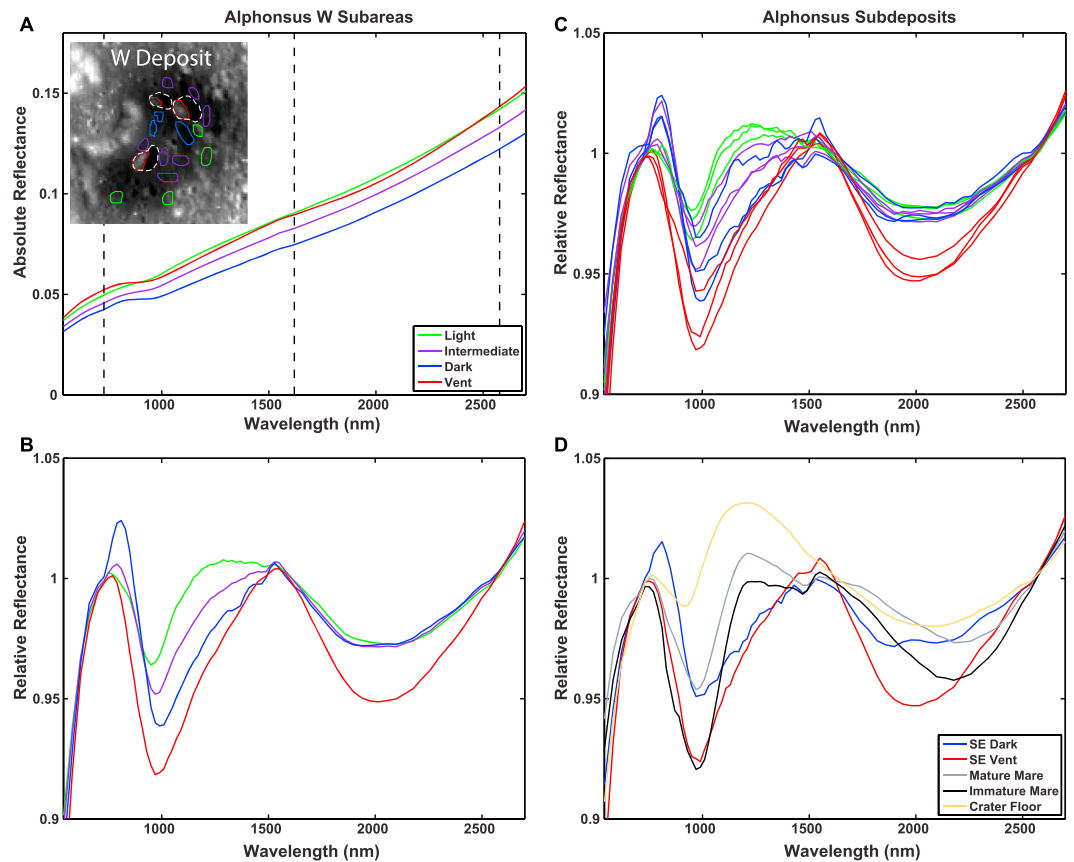


Figure 4. Spectra of Alphonsus crater DMDs. (a) Absolute reflectance of DMDs. Black dashed lines indicate the endpoints used to calculate the continuum. Inset image shows the study areas of each spectral unit (i.e., light, intermediate, dark, and vent) in the western subdeposit. Outline colors correspond to the colors in the spectra. White dashed lines are the approximate outline of the volcanic vents, while the spectral regions outlined in red are only the insolated portion used in the analysis. (b) Spectra from Figure 4a with continuum removal applied. (c) The continuum-removed spectra of the W, SE, and NE subdeposits in Alphonsus crater. The colors for the spectra are maintained from Figures 4a and 4b. (d) Continuum-removed spectra of SE deposit, as well as spectra from the floor of Alphonsus crater and two basalts from eastern Mare Nubium; see Figure 2. All spectra are smoothed as discussed in the text.

These absorptions are characteristic of mafic minerals such as pyroxene or Fe-bearing glass, when compared to the relatively less mafic-rich mineralogy of the highlands materials of the crater floor. An additional distinguishing factor between these units is differences in exposure age and the extent of space weathering—as noted above, an increased degree of space weathering will decrease the albedo and absorption band depths of a surface, which can also contribute to differences in these color maps.

There are notable variations in albedo from the volcanic vent to the distal edges of each subdeposit (Figure 3). As discussed in the previous section, the analysis of spectral features was restricted to band shape and position when comparing spectra from different optical periods, as variations in viewing geometry exist between different optical periods. However, albedo analyses are robust when comparing data from the same optical period, such as those within Alphonsus crater. Therefore, average spectra of the subdeposits were taken to examine this albedo variation trend. The unit names (light, intermediate, dark, and vent) indicate variations in albedo in the DMD, and these unit names were maintained across all subdeposits in Alphonsus crater. The absolute reflectance of the DMD is variable between the vent and near-vent DMD material and distal edges of the deposit (Figure 4a). This variation in albedo is not directly related to distance from the volcanic vent in all subdeposits, so the spectral units were drawn based on albedo variations rather than distance from the vent.

The vent units throughout Alphonsus crater have higher albedo values and deeper absorption bands than the other units (Figure 4). Previous studies suggested that bright material visible in the vents is due to

mass-wasting exposing high-albedo highlands material [Allen *et al.*, 2013]. This may be the reason for elevated albedo within the vents, while the deep absorption bands in the vent units may occur due to mass-wasting exposing fresh mafic materials on the steeper slopes of the vent. A second possibility is that these spectra include insolated portions of the vent walls (see inset of Figure 4a), where local incidence angles are higher than the surrounding flatter terrain. This incidence angle variation (not included at this resolution in the photometric correction) results in a higher signal-to-noise ratio received by the spacecraft, which acts to elevate the albedo and deepen the absorption bands. However, variations in topography have been calculated to change reflectance values by as much as 10% [Domingue and Vilas, 2007], which would not necessarily explain the variation in spectra within and outside the vents. Therefore, a variation in exposure ages due to space weathering and mass wasting inside the vent is favored over a purely photometric component.

Analyses within each of the subdeposits show variable spectral signatures related to the albedo variations discussed above. Spectra of the Alphonsus DMDs generally have very shallow absorption bands centered between 950–1020 nm and 2000 nm (Figure 4a). In the continuum-removed spectra, the 1 μm bands shift to shorter wavelengths and shallower absorption depths as albedo increases, while the position of the 2 μm band does not change with albedo (Figure 4b). These trends are seen among all the Alphonsus subdeposits, in particular in the transition from the dark to light units (Figure 4c).

The Alphonsus DMD mantles higher-albedo crater floor material, which is noritic in composition [Allen *et al.*, 2013] and less mafic than the DMDs which are relatively more rich in transition metals due to their stronger crystal field-splitting absorption bands [Burns, 1993]. This highland material displays a different band depth and position than the DMDs; a spectrum of the floor of Alphonsus crater (Figure 4d, “Crater Floor”) shows that the band center of the 1 μm band is located at 930 nm and the 2 μm band center is at \sim 2000 nm, suggesting a dominant component of low-calcium pyroxene. This spectrum appears convex at \sim 1.2 μm , which is expected to be a remnant of the continuum-removal process. It is important to note that the process of removing a spectral continuum can affect the shape of an absorption band, and the method of continuum-removal applied in this work (through using a linear continuum with fixed endpoints) may distort the shape of certain spectra. For example, spectra of surfaces with low 2 μm band centers or low interband peaks may become misshapen or demonstrate relative reflectance values greater than unity, as discussed in section 2.2. This convex feature in the crater floor spectrum is believed to be an artifact of this characteristic.

As spectra are examined in the lower albedo units, the 1 μm bands shift to longer wavelengths and deeper absorption depths. The spectra showing these shifts are not consistent with a low-calcium pyroxene mineralogy, suggesting a variation in mineralogy or internal structure of the DMD materials compared to the crater floor.

The shift in band position and absorption depth between the noritic crater floor and the more mafic DMDs is seen within each DMD subdeposit, as discussed above. This suggests that inside the vent, and in close proximity (i.e., the dark unit), spectra are dominated by mafic DMD materials. However, as distance from the vent increases toward the distal edges of the deposit (the light unit), spectra become contaminated by shorter- and shallower-wavelength noritic crater floor material. This variation is interpreted to represent a variable thickness across the DMD, manifested as varying areal mixtures at scales smaller than the spatial resolution of M^3 . While the deposit is thickest near the volcanic vent, the DMDs become more spectrally transparent near the distal edges of the deposit, causing the 1 μm band to shift to shorter wavelengths. Small-scale mixing and overall thinning of the deposit agrees with the increase in albedo across the units; as the DMD becomes more spectrally transparent, the bright crater floor material increases the albedo.

Additional spectra were taken in eastern Mare Nubium and divided into two units, “immature mare” and “mature mare” (see units labeled on Figure 2d). The immature mare unit is located in an area with a high concentration of small, young craters that exposed fresh, immature mare materials. This unit exhibits a strong 1 μm band centered at 970 nm and a weaker 2 μm band centered at 2220 nm, indicative of a high-calcium pyroxene. The mature mare unit is located in a region relatively free of fresh craters, and the spectrum is identical in band position to the immature mare unit but displays a shallower band depth. When compared to the spectra from the DMDs, there are differences in both band shape and position of the mare materials. The DMDs by comparison show a similar 1 μm band position but broader, asymmetric band shape and a slightly shorter 2 μm band position, relative to the maria, which are not consistent with this mineralogy. In general, the 1 μm bands of all the DMD spectra are broader in shape than the maria.

This distinction in spectra signifies a variation in either mineralogy or internal structure (i.e., crystallinity of the grains) between the two materials.

The DMDs are clearly mafic in composition, but the spectra are not consistent with a bulk mineralogy similar to either the low-calcium pyroxenes of the crater floor or the high-calcium pyroxenes of the mare basalts. The shape and locations of the DMD absorption bands suggest a component of pyroxene in the deposits, although pure pyroxene will not produce the asymmetries seen in these spectral bands. Previous analyses [e.g., *Hawke et al.*, 1989] characterized the wide, broad 1 μm absorption band in DMDs such as Alphonsus as indicative of olivine. However, the inclusion of olivine, or other mafic minerals, in the DMD would not explain the band center shifting to shorter wavelengths seen at 2 μm . It is possible that olivine may be present in the Alphonsus DMD, although another component is required to produce the observed 2 μm band position in the spectra. Fe-bearing glass has been observed to exhibit broad, shallow absorption bands with 1 μm bands shifted to longer wavelengths and 2 μm bands shifted to shorter wavelengths relative to pyroxenes [e.g., *Adams et al.*, 1974; *Horgan et al.*, 2014]. Therefore, this spectral signature may contain a component of amorphous materials in the form of iron-enriched volcanic glass. The glassy signature seen in the Alphonsus DMDs matches other DMDs which were recently identified as containing volcanic glass in *Besse et al.* [2014], as will be discussed in section 4.1.

3.2. J. Herschel Crater

J. Herschel crater is a 154 km diameter pre-Imbrian impact crater located in the highlands north of Mare Frigoris (Figure 1). The crater walls are heavily degraded, and a network of fractures is located on the eastern portion of the crater floor (Figure 5a and Table 2). The main DMD is located in conjunction with these floor fractures and contains several depressions located on and around the fractures which are interpreted to be volcanic vents [*Hawke and Head*, 1980]. Previous analyses have identified large juvenile components in the DMD in J. Herschel crater, containing highly mafic material including a mixture of olivine and pyroxene [*McCord et al.*, 1981; *Hawke et al.*, 1989; *Gaddis et al.*, 2000].

Due to poor viewing conditions at high latitudes, including high phase angle ($\sim 66^\circ$, Table 1), M^3 data of the J. Herschel DMD have a lower signal-to-noise ratio relative to other regions in the same optical period (e.g., the Alphonsus crater DMD). Despite this lower signal-to-noise ratio, color composite maps can be used to distinguish DMDs from highlands materials due to their mafic signatures, as the DMDs demonstrate stronger mafic absorptions than the highlands (Figure 5b).

A spectrum of an insolated portion of the central vent wall displays a low reflectance relative to a portion of recently exposed mare basalt (Figure 5c, "vent" and "immature mare"). The continuum-removed spectrum shows a 1 μm band centered at slightly less than 1000 nm, with a broad shoulder at 1250 nm (Figure 5d), while the 2 μm band is centered at ~ 1950 nm. Spectra of the DMD outside the vent exhibit 1 μm bands centered at the same location as the vent, but the absorption depth of the 1 μm band decreases and the 1250 nm shoulder becomes less pronounced (Figure 5d). The 2 μm band absorption depth also decreases from the vent to the DMD.

Compared to the DMD spectra, a spectrum taken of the crater floor (Figure 5c) has a much higher reflectance. The continuum-removed spectrum shows a narrow 1 μm band that is shifted to slightly shorter wavelengths than the DMD, and a shallow, broad 2 μm band (Figure 5d). This spectrum also appears convex at 1.2 μm , similar to that of the Alphonsus crater floor, which is attributed to an artifact of the linear continuum removal process on spectra of surfaces containing low-calcium pyroxene.

A spectrum of recently exposed Mare Frigoris basalt was included as an additional comparison to the J. Herschel DMDs. The spectrum of this region shows an albedo similar to that of the DMD material (Figure 5c). The continuum-removed spectrum shows a narrow, deep 1 μm absorption band centered at the same location as the DMDs, but without the shoulder at 1250 nm. The 2 μm band of the immature mare unit has approximately the same absorption depth as the 2 μm band of the DMD but is centered at a longer wavelength (~ 2200 nm, as opposed to ~ 1950 nm).

The spectra from this localized DMD are characteristic of material containing a component of volcanic glass, similar to the spectra of the previous localized DMD in Alphonsus. The asymmetric 1 μm band and the 2 μm band centered at ~ 1950 nm of the vent unit are similar to the shifted 1 and 2 μm band center positions of the DMD in Alphonsus.

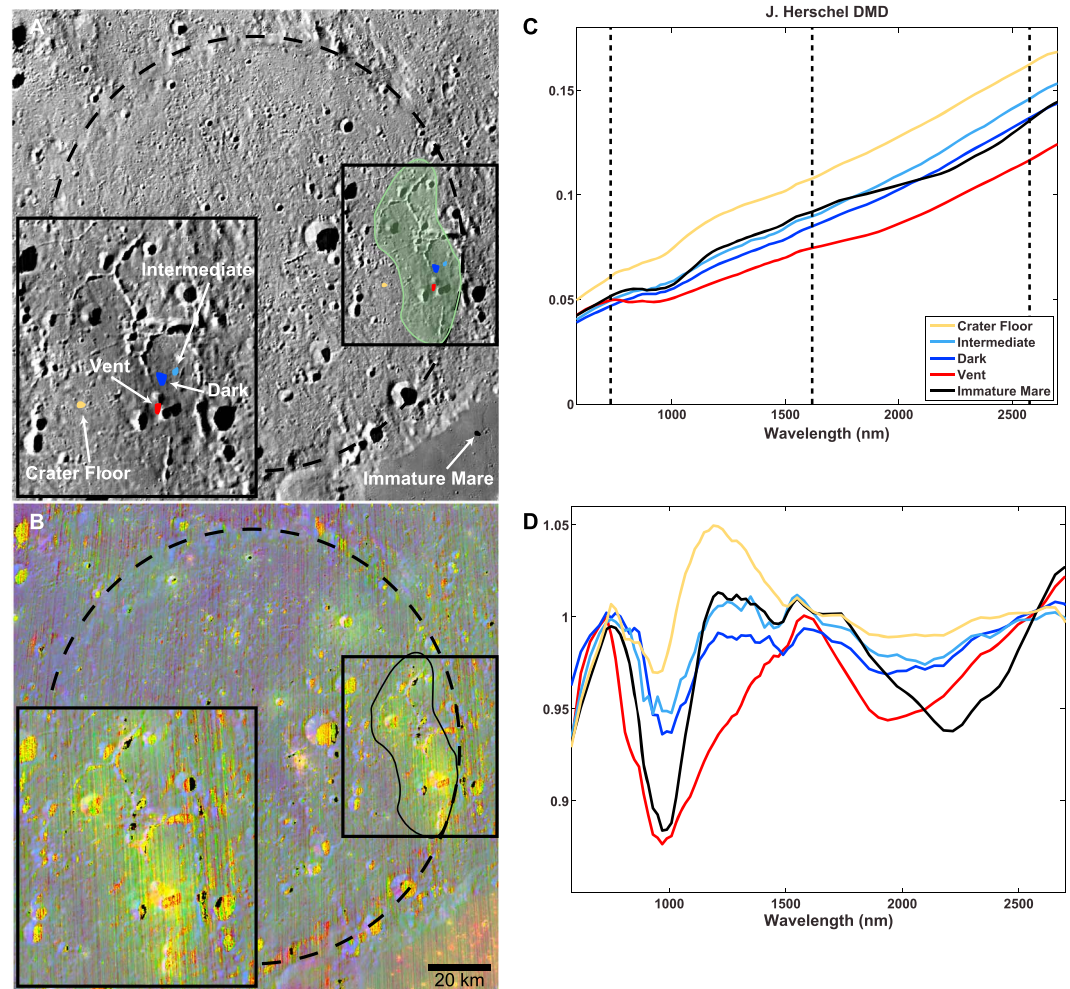


Figure 5. J. Herschel crater. (a) $1\ \mu\text{m}$ albedo map with DMD location outlined in green (see Table 2 for details). Inset: DMD with source areas for average spectra shown in Figure 5c. (b) RGB color composite image using R: IBD 1000 nm, G: BD 1900 nm, and B: R 1580 nm. Inset: zoom of the DMD as in Figure 5a. (c) Spectrum of areas outlined in Figure 5a, including DMD materials (intermediate, dark, and vent), and portions of the crater floor and mare basalt. Black dashed lines indicate the endpoints used to calculate the continuum. (d) Continuum-removed spectrum from Figure 5c. All spectra have been smoothed as discussed in the text.

As previously noted, the method of continuum removal applied in this work may incorrectly fit certain spectra, such as the highlands terrain. In addition, spectra with nonlinear slopes may also be improperly fit by this linear continuum (Figures 5c and 5d, “vent” unit). The distortion of absorption band shape and width can lead to mineralogical and compositional misidentification. However, the location of the 1 and $2\ \mu\text{m}$ band centers should not be affected largely by this, and the band shape can be trusted if compared against the original reflectance spectrum. Care should be taken when analyzing continuum-removed spectra, as false band asymmetries can lead to the misidentification of glass. Identifying and interpreting glass in VIS-NIR spectra are discussed further in section 4.1.

As in the Alphonsus DMD, other workers have previously classified the spectral signature in this DMD as olivine-rich [McCord *et al.*, 1981; Hawke *et al.*, 1989]. However (as also seen in Alphonsus), the presence of olivine alone would not explain the asymmetries and the positions of the absorption bands at 1 and $2\ \mu\text{m}$. Therefore, while it is possible that an olivine component may be present, these spectra are interpreted to signify the presence of volcanic glass in the J. Herschel DMD.

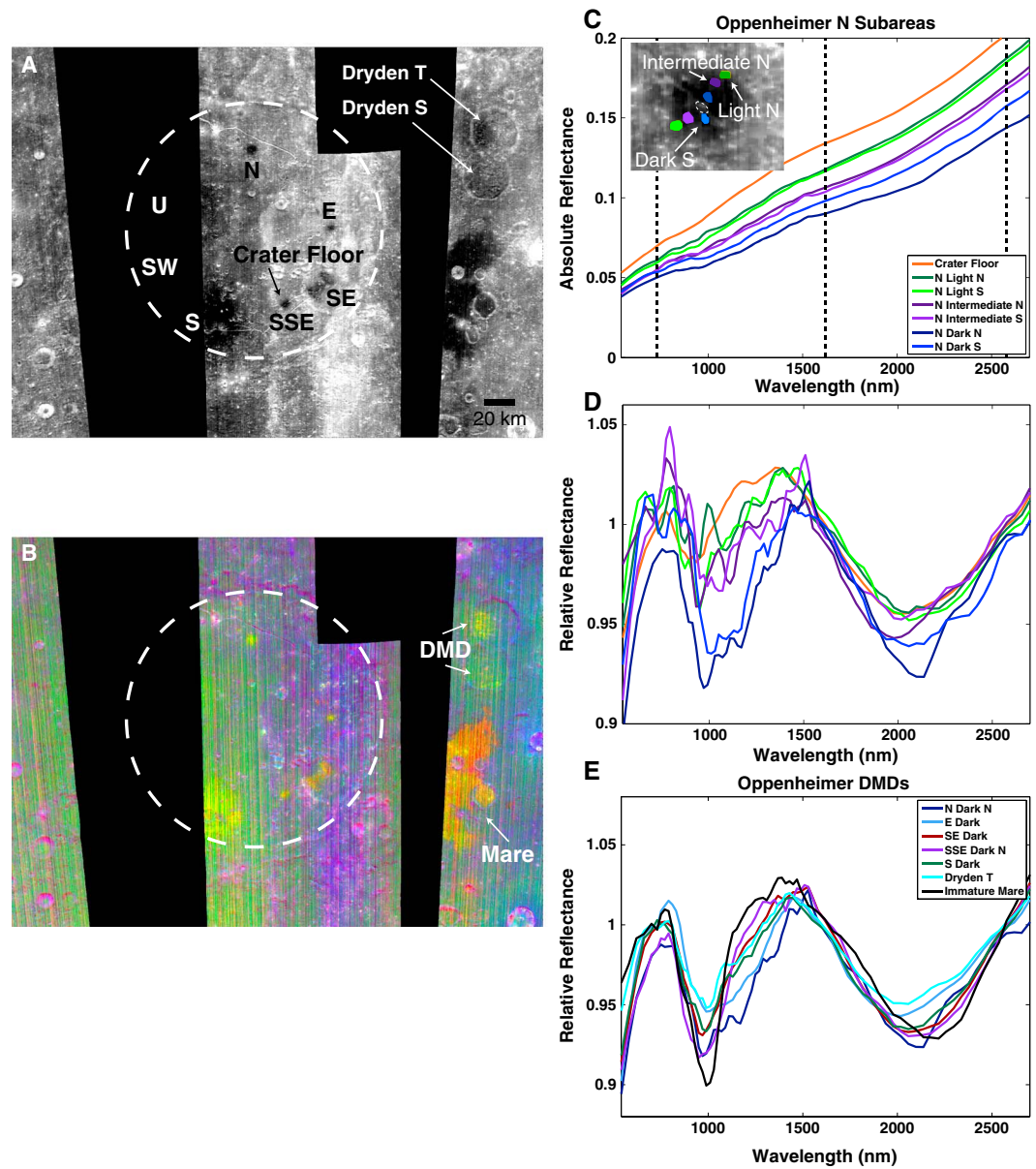


Figure 6. Oppenheimer crater. (a) 1 μm albedo map with labeled subdeposits after Gaddis et al. [2014] (see Table 2 for details). (b) RGB color composite image using R: IBD 1000 nm, G: BD 1900 nm, and B: R 1580 nm. (c) Absolute reflectance of the N subdeposit and Oppenheimer crater floor. Black dashed lines indicate the endpoints used to calculate the continuum. Inset: outlines of spectral units in the N subdeposit. White dashed line is the approximate outline of volcanic vent. (d) Continuum-removed spectrum of N subdeposit and crater floor. (e) Continuum-removed spectra of all Oppenheimer subdeposits and mare basalt. Also included is a spectrum of the Dryden T DMD material. All spectra have been smoothed as discussed in the text.

3.3. Oppenheimer Crater

Oppenheimer is a 201 km diameter pre-Nectarian floor-fractured impact crater on the lunar far side (Figure 1). The DMDs located around volcanic vents approximately coincide with the fractures on the crater floor. At least seven separate subdeposits are present across the crater [Rosanova et al., 1998; Head et al., 2000; Petro et al., 2001] (Figures 6a and 6b). Oppenheimer subdeposits SW and U are not covered by M^3 , although the available data coverage was favorable for this analysis as it included the other subdeposits throughout the crater, as well as the proximal mare deposit, within the same optical period. Oppenheimer crater

Table 3. Absorption Band Depth Ratios for the DMDs Analyzed^a

Glass/DMD	2/1 μm Band Depth Ratio	
	>0.67	<0.67
Orange Glass	0.80	
Green Glass		0.35
Alphonsus DMD		0.57
J. Herschel DMD		0.55
Oppenheimer DMD	0.89	
Walther A DMD	0.84	
Alphonsus Mature Mare		0.54
Alphonsus Immature Mare		0.58

^aBand depth ratios are calculated from the maximum absorption depth of the 2 μm band relative to the maximum absorption depth of the 1 μm band in the continuum-removed spectra. The two columns distinguish between high and low values to better highlight the difference in band ratio values. The spectra are taken from the following spectral units: Alphonsus SE Dark, Herschel Dark, and Oppenheimer N Dark N as defined in Figures 4–6 and Walther C-s from Figure 7 in Besse *et al.* [2014].

itself is located just west of the large Apollo multi-ring basin (151.5°W, 35.7°S, 524 km diameter), which contains deposits of mare material whose composition can be directly compared to the DMDs.

Spectra were taken of each subdeposit in Oppenheimer based on albedo variations, similar to the approach used in the Alphonsus DMD. The same naming scheme was used (light, intermediate, and dark) as those discussed previously. In the north and south-southeast deposits, these measurements were taken in two different and opposite directions in order to increase the robustness of the analysis (Figure 6c).

Albedo profiles of the north and south-southeast subdeposits show an increase

in reflectance with distance from the vent (Figure 6c), similar to Alphonsus. The vents in the Oppenheimer DMD are slightly smaller, $\sim 3 \text{ km}^2$, compared to the largest three vents in the Alphonsus DMD analyzed in this work (W, SE, and NE), which are on average $\sim 3.7 \text{ km}^2$. The variation in vent size and DMD areal extent (Table 2) may indicate compositional, mineralogical, and/or volatile variations between the deposits [Jozwiak *et al.*, 2015].

The continuum-removed spectra of the N subdeposit (Figure 6d) show 1 μm band minimum positions at $\sim 1000 \text{ nm}$ in the dark units, with shoulders at 1200 nm. The 2 μm band positions of these dark units are located at 2000–2100 nm. The intermediate and light units (Figure 6d) show a shift to slightly shorter and shallower 1 μm band positions at $\sim 950 \text{ nm}$ and a decrease in strength of the 1200 nm shoulder. The 2 μm bands of these units also decrease in absorption depth, although band positions remain relatively constant. These spectra are similar to the glass-bearing units seen in the previous two localized DMDs. The lack of variation in position of the 2 μm bands may be due to the similarity in band position between the pyroxene and glassy materials in the deposit.

As a comparison, a continuum-removed spectrum of the crater floor (Figure 6d) shows a 1 μm band at 930 nm, which is a similar location to the noritic spectrum of the Alphonsus and J. Herschel crater floors, as well as the convex feature at 1.2 μm in the continuum-removed spectra seen in the other spectra typical of low-calcium pyroxene-bearing units. Additionally, the 1 μm band position of this unit also appears to continue the trend of the 1 μm band shift toward shorter wavelengths from dark to light units (Figure 6d), as seen in Alphonsus. This trend seen in the northeast and south-southeast subdeposits suggests that there is thinning of the DMD with distance from the volcanic vent, similar to that observed in the Alphonsus DMDs. The transitions between units in the Oppenheimer crater DMDs are not as well defined as those seen in the Alphonsus subdeposits, although this may be attributed to the lower spatial resolution in the M³ OP2C data.

Spectra of the dark units from each Oppenheimer subdeposit show approximately uniform minimum position of the 1 μm band at 1000 nm (Figure 6e). However, the depth and asymmetry of the 1 μm absorption band vary between locations. In addition, the strength of the 2 μm band is approximately equal to that of the 1 μm band, yielding a 2/1 μm band ratio of the Oppenheimer DMD of ~ 0.89 (Table 3). This band ratio is distinct from the previous DMDs in Alphonsus and J. Herschel craters, where the 2/1 μm band ratios for both DMDs are ~ 0.56 . This may signify a compositional distinction in the volcanic glasses between these localized DMDs, which will be discussed in section 4.1.

A spectrum of recently exposed mare basalt in Apollo crater to the east (Figure 6e) shows a symmetric, deep absorption band at 1 μm , with a similar minimum 1 μm band position of the DMDs. The 2 μm band of the mare unit shows an absorption band at longer wavelengths, $\sim 2200 \text{ nm}$, relative to the DMDs.

The spectral variations across Oppenheimer and the mare basalts may be indicative of a glassy component in certain DMD subdeposits. If the strength of the 1200 nm shoulder combined with the shortening of the 2 μm

band is indicative of glass content, then the north and east subdeposits are interpreted to contain the highest glass content of the subdeposits analyzed. The south, southeast, and south-southeast subdeposits may also contain glassy material, but potentially in smaller quantities or concentrations than the north and east, due to the relative lack of a shoulder at 1200 nm and the shifting of the 2 μm bands to longer wavelengths.

These conclusions broadly agree with previous studies of volcanic glass content in Oppenheimer crater. *Bennett et al.* [2013] compared M^3 and Diviner data and concluded that the south, southeast, and south-southeast subdeposits are composed of a mixture of low-calcium pyroxene, country rock, and glass, while the south deposit shows a higher, more extensive glass concentration than the southeast and south-southeast. *Gaddis et al.* [2014] analyzed nine-band Multiband Imager (MI) data from the Kaguya spacecraft and concluded that the Oppenheimer U, southwest, and south subdeposits show a major component of a material such as iron-rich glass, while the southeast and south-southeast deposits are a less glass-rich mixture of low-calcium pyroxene and glass. They explain this difference as being due to the relative thinness of the southeast and south-southeast DMDs relative to the larger, lower-albedo Oppenheimer U deposit. These observations agree with the analyses from this study regarding the interpretation that the south subdeposit contains a glassy component and the southeast and south-southeast subdeposits contain a lesser glass component (the SSE subdeposit contains the weakest signature and may not contain any volcanic glass), but these previous studies did not discuss the glass component of the north or east subdeposits.

When observing the albedo and color maps of Oppenheimer crater, there appear to be additional DMD materials in two smaller craters, Dryden S and Dryden T, to the northeast of Oppenheimer crater (Figures 6a and 6b). The mare basalts, with strong absorptions at 1000 and ~ 2200 nm, will appear red-orange in the RGB map, while the DMDs have a stronger absorption at 1900 nm and appear more green-yellow in the RGB color map. Based on these characteristics, it is possible to identify two DMD-bearing craters to the northeast of the Oppenheimer crater (Figure 6b). A spectrum of this potential DMD shows a minimum 1 μm band position that is similar to the other Oppenheimer DMDs, as well as a slight shoulder at 1200 nm of similar strength to the south subdeposit (Figure 6e). The 2 μm band of the potential DMD is located at ~ 2000 nm, similar to that of the east subdeposit. These spectral data, combined with the lowered albedo and fine-grained, diffuse deposit morphology, suggest these are two new, previously unidentified localized dark mantle deposits in Dryden S and T craters. Spectra of these new DMDs suggest a similar composition to that in Oppenheimer crater, as well as a component of glass, further supporting the theory that volcanic glass is more widespread in localized DMDs on the Moon than is reported in the literature.

4. Discussion

4.1. Presence of Volcanic Glass

Spectral analyses of the various DMDs have permitted the identification of variations in mineralogy, deposit thickness, and crystallinity. Spectral signatures typical of volcanic glass-bearing units have been detected in all of the localized DMDs analyzed in this study. These glassy DMDs display the spectral characteristics typical of glassy material, compared to mare basalt (Figure 7a): an enhanced absorption at 1–1.5 μm creating a wide, asymmetric 1 μm absorption band that is located at or slightly above 1000 nm, as well as a 2 μm at or slightly below 2000 nm. Spectra from Walther A and Lavoisier DMDs supply two other DMDs to the inventory of floor-fractured craters from the literature [*Souchon et al.*, 2013; *Besse et al.*, 2014]. The Walther A spectrum also displays this glassy signature. However, the Lavoisier spectrum does not—the 1 and 2 μm band positions of the Lavoisier DMD fall closer to 970 and 2200 nm, respectively, which may indicate glass-free mafic material. The DMDs in Lavoisier could be associated with other effusive mafic flows, which suggests that the overall eruptive conditions at this crater may have been distinct from that in the DMDs in floor-fractured craters bearing glassy signatures, in that the eruption conditions changed from explosive to effusive throughout the emplacement of the deposit. This is distinct from the glassy DMDs, which appear to have only erupted explosively.

As an additional, more robust analysis of the DMD spectra, the 1 and 2 μm band centers for all of the key spectra discussed previously have been plotted against each other (Figure 8). These parameters were measured from the continuum-removed spectra, and band centers were found using the polynomial fitting technique discussed in section 2.2. The plotted spectra include the DMDs in Alphonsus (see Figure 4d), J. Herschel (see Figure 5d), Oppenheimer (see Figure 6d), Walther A, and Lavoisier (see Figure 7a) craters;

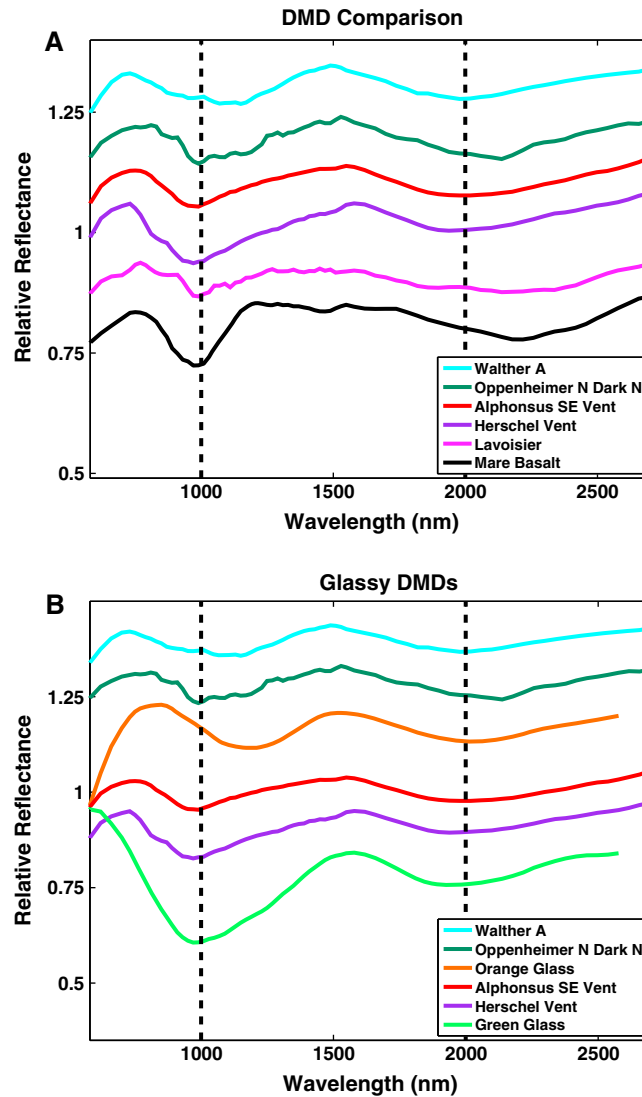


Figure 7. (a) Continuum-removed spectral comparison of the variation in the DMDs analyzed, including the Walther A and Lavoisier DMDs [Souchon et al., 2013; Besse et al., 2014] relative to mare basalt from Mare Frigoris, near the J. Herschel DMD (Walther C-s from Figure 7 in Besse et al. [2014], and Lavoisier PD from Figure 10 in Souchon et al. [2013]). (b) Continuum-removed spectra of the DMDs believed to contain glass, relative to laboratory spectra of lunar pyroclastic orange glass from the Apollo 17 landing site, sample 74220 [Adams et al., 1974] and green glass from the Apollo 15 sample 15401 [Pieters et al., 2000]. All spectra are offset for clarity, and M^3 data have been smoothed as discussed in the text.

orange glass and green glass (see Figure 7b), from Adams et al. [1974] and Pieters et al. [2000], respectively; and mare basalt (see Figure 4d) from Mare Nubium to the west of Alphonsus crater, as well as mare basalts from Oceanus Procellarum of varying ages and titanium contents [Staid et al., 2011]. The method of continuum removal applied in this work improperly fits certain spectral features, specifically low-calcium pyroxene-rich lithologies seen in the floors of the three craters, as discussed above (see Figures 4d, 5d, and 6d). For this reason, these spectra have not been included in the discussion of band centers and relative band depths; the spectra included in this analysis are those believed to be properly fit by the continuum removal. In addition, laboratory spectra of several mineral mixtures were plotted to show the possible range of band center positions one would expect from mafic lunar targets. These data include mixtures of pyroxenes (orthopyroxene and clinopyroxene), olivine, and glass [Horgan et al., 2014]. These mixtures encompass a wide range of spectral parameter space, and each mixture indicates a distinct geologic history. Shaded regions have been drawn to indicate the general region of band centers typical of orthopyroxene (OPX), clinopyroxene (CPX), and glass, after Horgan et al. [2014], as well as a region of typical mare basalts, after Besse et al. [2014].

The laboratory data shown in Figure 8 connected by broken lines describe the shift of the absorption bands at varying mafic mixture concentrations [see Horgan et al., 2014, for the individual spectra]. As can be seen, the mixtures of pyroxenes (open circles and closed circles) follow a fairly linear mixing trend between the CPX and

OPX regions; the majority of the data points in the mare basalts region lie within this CPX region as well, while mixtures of pyroxenes and glasses (open squares and diamonds) follow somewhat linear trends between the pyroxene and glass regions. Mixtures of orthopyroxene and olivine show a nonlinear increase in the 1 and 2 μm band centers with increasing olivine content. However, olivine does not exhibit a diagnostic 2 μm absorption band, so at high olivine concentrations, the 2 μm band data become noisy due to the weak pyroxene absorptions, relative to the more orthopyroxene-rich data.

The remotely sensed spectra of the localized DMDs plot in three distinct regions: Walther A, within the glass region; Oppenheimer and Lavoisier, within the mare basalt/CPX region; and Alphonsus and Herschel, above

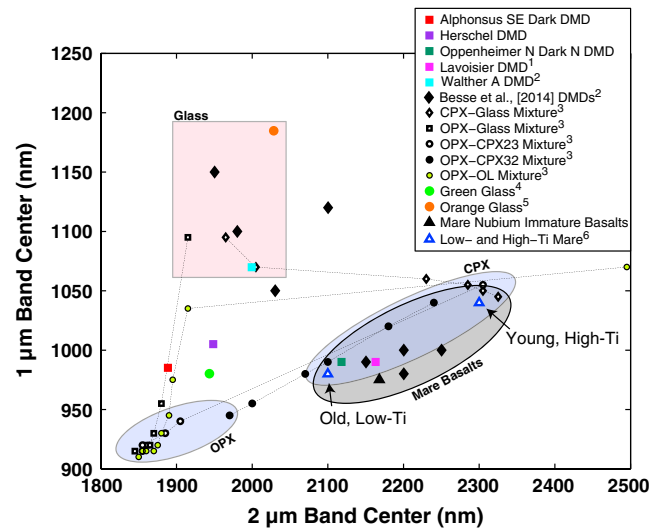


Figure 8. Band center position at 1 and 2 μm . The band center was assumed to be the location of the band minimum as discussed in the text. Spectral parameters from Alphonse, Herschel, and Oppenheimer DMDs are plotted. Additional data from the literature are also included: Lavoisier [Souchon *et al.*, 2013]; Walther A and additional glass-bearing and glass-free DMDs [Besse *et al.*, 2014]; mixtures of various mafic minerals (CPX-glass: PYX016_TEK004_It45; OPX-glass: PYX023_TEK004_It45; OPX-CPX23: PYX23_PYX005_It45; OPX-CPX32: PYX032_PYX017_It45; OPX-OL: PYX042_OLV003_38-53) [Horgan *et al.*, 2014]; Apollo 15 green glass [Pieters *et al.*, 2000]; Apollo 17 orange glass [Adams *et al.*, 1974]; and old, low-Ti mare basalts and young, high-Ti mare basalts within Oceanus Procellarum from Staid *et al.* [2011]. The shaded regions for OPX and CPX (blue) and glass (pink) reflect those from Figure 11 in Horgan *et al.* [2014], while the Mare Basalt region (grey) reflects that from Figure 9 in Besse *et al.* [2014]. Note that the Alphonse, J. Herschel, and green glass band positions are in close proximity to that of mixtures of both OPX and glass, and OPX and olivine, although high concentrations of either glass or olivine would be required. The band positions of the Oppenheimer and Lavoisier DMDs plot within the mare basalt region, although the band position parameter is not sensitive to band asymmetries or relative 2/1 μm band absorption strengths (see Table 3), which suggests there may be glass present in the Oppenheimer DMD.

of the DMDs and the green glass spectra. It is impossible to rule out the possibility of a component of olivine, and this mineral may be present, but a glassy component is expected in both the Alphonse and J. Herschel DMDs.

As discussed in Besse *et al.* [2014], several of the DMDs analyzed in that work, including Walther A, plot in the glass region near the orange glass, suggesting a large component of volcanic glass in these deposits. However, the Oppenheimer DMD, which is argued in section 3.3 to contain volcanic glass, plots well within the mare basalt range, near the Lavoisier DMD spectrum. This discrepancy in band position of the Oppenheimer DMD may be credited to the fact that there is a stronger pyroxene component, and the band center parameter does not completely account for band asymmetries or relative absorption band strength.

The localized lunar DMDs are understood to be emplaced in explosive, transient vulcanian-style eruptions (see section 4.3). The nature of this eruptive style is such that country rock, entrained in the erupting magma [e.g., Head and Wilson, 1979], could be present within the deposits and may contribute to band center locations discussed above. Specifically, this potential highlands component may affect the 1 μm band center positions of the DMD spectra: highlands typically contain a 1 μm band center around $\sim 950\text{ nm}$; in addition, mature highland spectra generally do not have strong 2 μm absorption bands (e.g., Figure 5c). Based on these two spectral properties, mixtures of DMD and highlands materials may cause 1 μm band center positions to move downward in Figure 8 (the highlands region in the band center plot would lie near the OPX region in Figure 8). Furthermore, the weak 2 μm band in highlands spectra should not move the DMD points laterally in Figure 8.

the OPX but below the glass region. The green glass also plots within this region. The mixing trends shown in Figure 8 suggest that this region encompasses mixtures of orthopyroxene, glass, and olivine. This suggests that the spectra taken at Alphonse and J. Herschel may be mixtures of pyroxene and glass or pyroxene and olivine (or mixtures of all three). However, the laboratory spectrum of green glass, which also plots in this region, contains no olivine or pyroxene. Furthermore, to occupy this region, mixtures with orthopyroxene would require $\sim 80\text{--}90\%$ olivine or glass [Horgan *et al.*, 2014]. Given the DMD setting, an olivine concentration of 80–90% would be unlikely, while large concentrations of glass is possible given the geologic setting.

Therefore, while the spectral data suggest a mixture of low-calcium pyroxene and either glass or olivine, a LCP-glass mixture is expected; while mixtures of low-calcium pyroxene and olivine cannot be ruled out spectrally, this is petrologically unlikely. In addition, the shape and relative strength of the 2 μm absorption band in the Alphonse and J. Herschel spectra (Figure 7) suggest a glass component is necessary, rather than an olivine component, to create the DMD spectra. Therefore, assuming glass is present, it is likely to be compositionally similar to that of green glass, given the proximity of band centers of

As many as 25 different volcanic glasses have been identified in the lunar sample collection (clear, yellow, orange, red, green, and brown); these vary in color due to compositional distinctions and degree of crystallinity [Delano, 1986; Gaddis *et al.*, 2003]. In addition to the glasses, black beads were detected via telescopic observations and were later measured in the laboratory [Pieters *et al.*, 1973; Adams *et al.*, 1974; Weitz *et al.*, 1999]. Both the black beads and orange glass have been identified at the Apollo 17 landing site in the Taurus-Littrow Valley from analyses of returned lunar samples. Green glass was returned from the Apollo 15 landing site but has not been remotely detected in large quantities in other locations [Gaddis *et al.*, 2003]. The black beads have been shown to be composed of crystalline, iron-rich, and ilmenite-rich material and represent the crystalline equivalents of the orange glass [Heiken *et al.*, 1974]. The green glass varies in composition but is generally iron-rich, less titanium-rich than the orange glass, and amorphous in internal structure and contains a component of olivine [Delano, 1979].

The relative strength of the 1 and 2 μm absorption bands, referred to as the 2/1 μm band ratio, has been observed to vary between green and orange lunar glasses; green glass shows a 2/1 μm band ratio of 0.35 (i.e., the 1 μm band absorption depth is deeper than the 2 μm band), while the band ratio for orange glass is 0.80 (i.e., the 1 and 2 μm band absorption depths are approximately equal) (Table 3) [Adams *et al.*, 1974; Gaddis *et al.*, 2003]. In addition, the 1 μm band of orange glass is approximately symmetric, while the 1 μm band of green glass is asymmetric, showing a shoulder at ~ 1250 nm (Figure 7b).

The spectra collected in this work represent mixtures of minerals within the DMDs, including crystalline and glassy materials; the glass component in these spectra is expected to change the band depth ratio to varying extents, which may be diagnostic of the glass composition. In these data, the Oppenheimer band ratio is 0.89, very similar to that of the orange glass and Walther A band ratios, which are 0.80 and 0.85, respectively. When compared to the 2/1 μm band ratio values of orange and green glass, the Alphonsus and J. Herschel DMD values are closer to the band ratio of green glass, 0.35. This suggests the glass in the Alphonsus and J. Herschel DMDs may be compositionally similar to green glass: the shapes of the 1 μm band in these spectra are also asymmetrical, with a shoulder at ~ 1250 nm, similar to the spectrum of green glass. The Oppenheimer DMD spectra, while showing a similar band ratio to that of orange glass, are also characterized by an asymmetric 1 μm band similar in shape to the other glassy spectra, rather than the more symmetric 1 μm band of orange glass.

Through a combination of the two spectral parameters discussed above, band center position and 2/1 μm band ratio, it is possible to identify the presence of glass in the DMDs. Both parameters are required in order to confirm the presence of glass, as each of these parameters may be ambiguous on its own; for example, the Oppenheimer DMD appeared to plot well within the mare basalt region of the band position plot (Figure 8), while the 2/1 μm band ratio (Table 3) suggests the strength of the absorption bands was less similar to mare basalt and more similar to orange glass. This is possible if the absorption bands are asymmetric, or if they contain a component of material of a different crystallinity to change the absorption band depth relative to surrounding material. Conversely, the Alphonsus and J. Herschel DMD 2/1 μm band ratio values were almost identical to that of the mare basalts, although their band positions are less similar to mare basalts, and more similar to that of green glass. Therefore, both metrics are necessary in order to prevent misclassifying glass contributions, and are useful in classifying and distinguishing DMDs.

Previous DMD classifications used the presence of olivine as a distinguishing characteristic, which comprised "Group 3" DMDs in Hawke *et al.* [1989]. These deposits (including Alphonsus and J. Herschel DMDs) displayed an asymmetric 1 μm band, often with a broad shoulder located ~ 1200 – 1250 nm. This 1250 nm feature was likewise visible in the spectra described in this work of both the Alphonsus and J. Herschel DMDs (Figures 4 and 5). A shoulder at 1250 nm is typical of olivine-bearing units, as well as a weak or absent 2 μm band, although it has been shown that spectra of Fe-bearing olivine compositions can be indistinguishable from low-calcium pyroxene mixed with Fe-bearing glass [Horgan *et al.*, 2014]. Therefore, in general, spectra that contain the diagnostic features of olivine may in fact contain a more complex mixture of minerals of which iron-bearing glass may be a component. Detailed spectral deconvolutions are required in order to quantify the abundance of these contributing factors.

Previous work by Tompkins and Pieters [2010] has shown that it is not possible to distinguish between volcanic glass and impact melt glass from spectra alone. However, consideration of several other factors, such as geologic context, makes it possible to distinguish volcanic from impact-generated glasses. In the locations studied in this work, specifically the localized DMDs in floor-fractured craters, glassy signatures occurred solely

in deposits of low-albedo, mafic material in close proximity to volcanic vents. Moreover, in multiple locations, the glassy spectral signature weakened as distance from the volcanic vent increased, implying that the glass is sourced from the volcanic vent. While impact melt glass is likely to be present on the crater floor, and a component of this may be mixed with the DMDs, the concentration of impact-generated glass would not be high enough to be detected in the spectra. This is supported by the weakening glass signature in the spectra with increasing distance from the volcanic vent, as it appears that a high concentration of glassy materials is necessary in order to create a detectable spectral signature.

In addition, the probing depth of VIS-NIR spectra is limited to the upper microns of the surface; this prevents any spectral contribution from a glass-bearing impact melt substrate related to the host crater formation, as the DMDs are emplaced on top of the impact melt after it has solidified. Mixing is observed with the substrate at the distal edges of the deposits, but these are the locations of the weakest glass detections. Therefore, it is possible to conclude with certainty that the glassy signatures detected in this work are volcanically generated and not impact-related glass.

4.2. Variations in DMDs

Variations were detected across the various subdeposits in the Alphonsus crater DMD. The variations in albedo and 1 μm band position and depth are consistent with a transition from mafic to noritic materials, suggesting a thinning of the DMD toward its distal edges. As the deposit becomes thinner at the edges, mixing with the substrate becomes more pronounced. This thinning/mixing relationship helps to explain the spectral transition from DMD to crater floor seen in the Alphonsus DMD.

This thinning is also seen in the small, isolated deposits in the Oppenheimer DMD. The same trend is not as clearly observed in the J. Herschel DMD, although the variation in albedo supports a similar thinning and areal mixing as has been interpreted in Alphonsus and J. Herschel. Multiple factors may be credited for this, including the fact that the substrate is believed to be spectrally similar in band center position to that of the DMD, so the spectral variation is not expected to be as large as that seen in the Alphonsus and Oppenheimer DMDs. In addition, the high latitude of J. Herschel crater and therefore high phase angle reduces the signal-to-noise ratio of the data, which may have contributed to the less distinguishable thinning/mixing trend.

Due to this thinning, and the variation in spectra across the DMDs, caution should be taken when measuring average spectra of subdeposits; the inclusion of the thin, distal edges of these isolated deposits may skew the band depth and positions of the resulting spectra. Variations in spectral signatures have been identified previously in the Alphonsus DMD [Robinson *et al.*, 1996], although thinning of the DMD was not proposed as a mechanism to explain this. Rather, the variation seen in the individual subdeposits was taken to suggest variations in eruption style, duration, the addition of a country rock component in the DMD [Head and Wilson, 1979], etc., suggesting mineralogical diversity within the deposits.

In addition to variations in deposit thickness with distance from the vent, the glassy component of the DMD may vary with distance as well. For example, in all three localized DMDs, the strength of the 1 μm band asymmetry decreases with distance from the central vent (compare dark and intermediate or light spectra in each DMD). The shift in 1 μm band center positions suggests variations in deposit mineralogy, as discussed in relation to thinning above, but the variation in band asymmetry is more expected to be due to variations in crystallinity. In light of this observation, the DMDs are in general more glass-rich in close proximity to their central vents, transitioning to less glassy or more crystalline materials at the distal margins of the deposits. The implications this has on emplacement mechanisms are discussed in the following section.

Spectral variations between DMDs and mare basalts were seen in all locations. In general, the mare basalt spectra are shifted to slightly shorter 1 μm band positions and longer 2 μm band positions, relative to the DMDs (Figures 4d, 5d, and 6e). The 1 μm bands of the mare are more symmetric, lacking shoulders ~1200–1250 nm, which are present in most of the DMD spectra, and the 2/1 μm band ratios of the mare basalts are all <0.6. These mare spectra are broadly indicative of the presence of high-calcium pyroxene.

4.3. Emplacement Style

The general eruptive model for localized DMDs proposed by [Head and Wilson, 1979] envisions a dike emplacement event in association with the fractures on the crater floor, buildup of gas at the top of the

dike, and an explosive, vulcanian-style eruption that incorporates country rock, disrupted and rapidly cooled magmatic foam to form glass beads, and incorporated magma from the top of the dike to form crystalline spatter. The large areal extent of the deposit around the volcanic vent, the relatively flat topography of the dark mantle deposit, the size of the vents, their location along fractures, and the lack of volcanic constructs and associated lava flows all favor a vulcanian eruption style, rather than a strombolian or hawaiian style [Head and Wilson, 1979, 1992]. The fractures in floor-fractured craters, such as the ones analyzed in the three craters in this study, are believed to form through magmatic intrusion under the crater floor [Schultz, 1976]. The fractures can act as conduits for volatiles and magma to reach the surface. When the magma in the tip of the dike nears the surface, it cools and pressure builds up behind a cooled plug or caprock due to volatile accumulation in the magma; ultimately, the pressure exceeds the tensile strength of the plug [Head and Wilson, 1979]. At this point, the volatile foam and liquid magma droplets are ejected rapidly, creating a gas-rich explosive expanding hemisphere. The explosive nature of the eruption will entrain wall rock and other nonjuvenile components with the ejected magma. The resulting deposit is approximately centered around the volcanic vent and is rich in crystalline and amorphous mafic material with a component of nonjuvenile (wall rock) material.

The detection of glassy material in the localized DMDs analyzed in this study supports an eruption model where travel times and optical densities of the volcanic eruptions were relatively low. This agrees with the model of vulcanian-style eruptions for localized deposits, as opposed to more long-duration hawaiian-style eruptions believed to have created the larger regional DMDs. In addition, there is evidence for a higher concentration of volcanic glass in close proximity to the volcanic vent, as discussed in the previous section. This is the opposite observation of what is observed in returned cores from the Apollo 17 landing site containing orange glass and black beads [Weitz *et al.*, 1999]. These returned samples suggested that crystalline materials (i.e., black beads) were more prominent closer to the eruptive center, where optical density was higher and crystallization was encouraged; in contrast, amorphous materials (i.e., orange glass) were more prominent at greater distances from the vent, where the lower optical density and temperature present in the outer parts of the eruptive plume were conducive to more rapid quenching. If the localized DMDs were emplaced in a similar eruptive manner to the regional deposits, glass would not be expected in close proximity to the volcanic vent. This signature is therefore evidence that the localized DMDs were emplaced in a smaller, faster, and otherwise cooler eruptive style than the regional DMDs.

A second possible explanation for elevated glass concentrations in close proximity to the vents is that multiple eruptions occur through the same volcanic vent. As volatiles are released through magma degassing in each eruption, the overall volatile content of the magma decreases. Each subsequent eruption would emplace volcanic glass at the distal edges of the new deposit in a similar manner to the first eruption. However, as the magma becomes more depleted in volatiles, the eruptive plumes would decrease in areal extent. In this manner, glassy material could be concentrated at locations closer to the central vent in each subsequent eruption, leading to a stronger glassy spectral signature around the volcanic vent. Multiple eruptions such as the one detailed here have been proposed on Mercury [Rothery *et al.*, 2014].

The variable spectra in several localized DMDs suggest the concentrations of both olivine and glass are not consistent across the lunar surface. Therefore, the groups created by Hawke *et al.* [1989] need to be modified, as these groupings do not at present distinguish DMDs based on the presence of glass. Therefore, modifications to the group classifications may be necessary [Besse *et al.*, 2014] in order to distinguish DMDs with glass and without glass, as well as variations in DMD composition.

5. Conclusions

Three localized dark mantle deposits (Alphonsus, J. Herschel, and Oppenheimer craters) were analyzed in order to compare variations in mineralogy and internal structure (i.e., crystallinity) across the lunar surface. All of the DMDs showed mafic absorption features that were distinguishable from surrounding mare basalt units. All the localized DMDs showed spectral signatures consistent with the presence of a volcanic glass component, which may be quite abundant in certain DMDs. This signature agrees with previous detections of volcanic glass in other localized DMDs by Besse *et al.* [2014].

The glassy spectral signatures of the DMDs suggest that glasses similar in composition to the Apollo orange and green glasses are present in varying quantities. Two new DMDs were also identified to the northeast of Oppenheimer crater in Dryden S and T craters. Variations in 1 μm band position and depth were observed in

both the Alphonsus and Oppenheimer DMDs, signifying a variation in deposit thickness toward the distal edges of the individual subdeposits. Caution should be taken when analyzing averaged DMD spectra, as the inclusion of the distal edges of these deposits may affect the spectral signatures due to the inclusion of adjacent or admixed highlands components.

The spectral detection of glass supports the model of a vulcanian-style eruption mechanism for the localized DMDs analyzed in this work. The eruptive conditions present in vulcanian-style eruptions lead to lower optical densities and temperatures than the hawaiian-style eruptions interpreted to be more typical of regional DMD emplacement. The lower optical densities and temperatures lead to rapid cooling, yielding a component of amorphous volcanic glass in the final deposit which is similar to that observed and documented in this study.

This study represents the next step in identifying volcanic glass in lunar dark mantle deposits, although additional progress is needed in several areas. Additional mafic lunar glasses could be introduced to the analysis to more adequately assess the composition of the localized DMD volcanic glass. The global population of DMDs must be inspected for volcanic glass signatures in a manner similar to this analysis and those by Besse *et al.* [2014] and Horgan *et al.* [2014]. Spectral modeling of the volcanic glass will also provide more detailed constraints on the emplacement, the distribution across various DMDs, and the mineralogical mixtures present in these deposits. Additionally, correlation with data from other instruments will yield a more complete analysis of these deposits [e.g., Trang *et al.*, 2014]. For example, incorporation of data from the Diviner instrument [Paige *et al.*, 2010] will allow determinations to be made about surface block populations, thermal properties, and felsic components in these DMDs. In addition, radar data from ground-based observations from Arecibo [Campbell *et al.*, 2007] and spacecraft-based observations from the Mini-RF instrument [Nozette *et al.*, 2010] can reveal the population of surface and subsurface scattering materials in the DMDs. The incorporation of these two data sets can help constrain DMD grain size and mineralogical variations and lead to improved understanding of the eruption mechanics operating in the formation of these deposits.

Acknowledgments

We would like to thank the Faculty Council at ESTEC for providing research support for the duration of this project. Thoughtful reviews provided by Briony Horgan and two anonymous reviewers were greatly appreciated and helped in improving the manuscript. The ESA fellowship program supported the research of S. Besse. L. R. Gaddis was supported by an award from the NASA Planetary Geology and Geophysics program. Support was provided from the NASA Solar System Exploration Research Virtual Institute (SSERVI) for J. W. Head. Users can access the data from this paper via the Planetary Data System Geosciences Node, <http://pds-geosciences.wustl.edu/>, from the M³ Archives, data set name: CH1M3_0004. The specific data files used to create the mosaics in this work are listed in Table 1.

References

- Adams, J. B., and T. B. McCord (1971), Optical properties of mineral separates, glass, and anorthositic fragments from Apollo mare samples, in *Proc. Lunar Sci. Conf. 2nd*, vol. 3, pp. 2183–2195, The M.I.T. Press, Cambridge, Mass.
- Adams, J. B., C. Pieters, and T. B. McCord (1974), Orange glass: Evidence for regional deposits of pyroclastic origin on the moon, in *Proc. Lunar Conf. 5th, Suppl. 5 Geochim. et Cosmochim. Acta.*, pp. 171–186, Pergamon Press, New York.
- Allen, C. C., K. L. Donaldson Hanna, C. M. Pieters, D. P. Moriarty, B. T. Greenhagen, K. A. Bennett, G. Y. Kramer, and D. A. Paige (2013), Pyroclastic deposits in floor-fractured craters—A unique style of lunar basaltic volcanism?, *Lunar Planet. Sci. Conf. 44th*, Abstract 1220.
- Bell, P. M., H. K. Mao, and R. A. Weeks (1976), Optical spectra and electron paramagnetic resonance of lunar and synthetic glasses: A study of the effects of controlled atmosphere, composition, and temperature, in *Proc. Lunar Sci. Conf. 7th*, vol. 3, pp. 2543–2559, Pergamon Press, New York.
- Bennett, K. A., B. H. N. Horgan, B. T. Greenhagen, and D. A. Paige (2013), Joint M³ and Diviner analysis of the mineralogy, glass composition, and country rock content of pyroclastic deposits in Oppenheimer Crater, poster presented at the Virtual Lunar Science Forum, NASA Lunar Science Institute.
- Besse, S., J. Sunshine, M. Staid, J. Boardman, C. Pieters, P. Guasqui, E. Malaret, S. McLaughlin, Y. Yokota, and J.-Y. Li (2013), A visible and near-infrared photometric correction for Moon Mineralogy Mapper (M3), *Icarus*, 222(1), 229–242, doi:10.1016/j.icarus.2012.10.036.
- Besse, S., J. M. Sunshine, and L. R. Gaddis (2014), Volcanic glass signatures in spectroscopic survey of newly proposed lunar pyroclastic deposits, *J. Geophys. Res. Planets*, 119, 355–372, doi:10.1002/2013JE004537.
- Boardman, J. W., C. M. Pieters, R. O. Green, S. R. Lundeen, P. Varanasi, J. Nettles, N. Petro, P. Isaacson, S. Besse, and L. A. Taylor (2011), Measuring moonlight: An overview of the spatial properties, lunar coverage, selenolocation, and related Level 1B products of the Moon Mineralogy Mapper, *J. Geophys. Res.*, 116, E00G14, doi:10.1029/2010JE003730.
- Burns, R. G. (1970), Site preferences of transition metal ions in silicate crystal structures, *Chem. Geol.*, 5(4), 275–283, doi:10.1016/0009-2541(70)90045-8.
- Burns, R. G. (1993), *Mineralogical Applications of Crystal Field Theory*, Cambridge Univ. Press, Cambridge, U. K.
- Campbell, B. A., D. B. Campbell, J. L. Margot, R. R. Ghent, M. Nolan, J. Chandler, L. M. Carter, and N. J. S. Stacy (2007), Focused 70-cm wavelength radar mapping of the Moon, *IEEE Trans. Geosci. Remote Sens.*, 45(12), 4032–4042, doi:10.1109/TGRS.2007.906582.
- Clark, R. N., C. M. Pieters, R. O. Green, J. W. Boardman, and N. E. Petro (2011), Thermal removal from near-infrared imaging spectroscopy data of the Moon, *J. Geophys. Res.*, 116, E00G16, doi:10.1029/2010JE003751.
- Cloutis, E. A. (2002), Pyroxene reflectance spectra: Minor absorption bands and effects of elemental substitutions, *J. Geophys. Res.*, 107(E6), 5039, doi:10.1029/2001JE001590.
- Cloutis, E. A., and M. J. Gaffey (1991), Pyroxene spectroscopy revisited: Spectral-compositional correlations and relationship to geothermometry, *J. Geophys. Res.*, 96(E5), 22,809–22,826, doi:10.1029/91JE02512.
- Cloutis, E. A., J. M. Sunshine, and R. V. Morris (2004), Spectral reflectance-compositional properties of spinels and chromites: Implications for planetary remote sensing and geothermometry, *Meteorit. Planet. Sci.*, 39(4), 545–565, doi:10.1111/j.1945-5100.2004.tb00918.x.
- Delano, J. W. (1979), Apollo 15 green glass—Chemistry and possible origin, in *Lunar and Planetary Science X*, pp. 275–300, Pergamon Press, New York.
- Delano, J. W. (1986), Pristine lunar glasses: Criteria, data, and implications, *J. Geophys. Res.*, 91(B4), 201–213, doi:10.1029/JB091iB04p0D201.
- Delano, J. W., and K. Livi (1981), Mare volcanic glass: A tale of two arrays, in *Lunar and Planetary Science XII*, pp. 226–228.

- Domingue, D., and F. Vilas (2007), Local topographic effects on photometry and reflectance spectra of planetary surfaces: An example based on lunar photometry, *Meteorit. Planet. Sci. Arch.*, *42*(10), 1801–1816.
- Duke, M. B., L. R. Gaddis, G. J. Taylor, and H. H. Schmitt (2006), Development of the Moon, *Rev. Mineral. Geochem.*, *60*(1), 597–655, doi:10.2138/rmg.2006.60.6.
- Elkins-Tanton, L. T., S. Burgess, and Q.-Z. Yin (2011), The lunar magma ocean: Reconciling the solidification process with lunar petrology and geochronology, *Earth Planet. Sci. Lett.*, *304*(3–4), 326–336, doi:10.1016/j.epsl.2011.02.004.
- Gaddis, L. R., C. M. Pieters, and B. Ray Hawke (1985), Remote sensing of lunar pyroclastic mantling deposits, *Icarus*, *61*(3), 461–489.
- Gaddis, L. R., B. R. Hawke, M. S. Robinson, and C. Coombs (2000), Compositional analyses of small lunar pyroclastic deposits using Clementine multispectral data, *J. Geophys. Res.*, *105*(E2), 4245–4262, doi:10.1029/1999JE001070.
- Gaddis, L. R., M. I. Staid, J. A. Tyburczy, B. R. Hawke, and N. E. Petro (2003), Compositional analyses of lunar pyroclastic deposits, *Icarus*, *161*(2), 262–280, doi:10.1016/S0019-1035(02)00036-2.
- Gaddis, L. R., S. Klem, J. O. Gustafson, B. R. Hawke, and T. A. Giguere (2011), Alphonsus dark-halo craters: Identification of additional volcanic vents, *Lunar Planet. Sci. Conf. 42nd*, Abstract 2691.
- Gaddis, L. R., J. Laura, B. Horgan, K. Bennett, B. R. Hawke, and T. Giguere (2014), Compositions of pyroclastic deposits in floor-fractured Oppenheimer crater, *Lunar Planet. Sci. Conf. 45th*, Abstract 2383.
- Gaffey, M. J., J. F. Bell, R. H. Brown, T. H. Burbine, J. L. Piatek, K. L. Reed, and D. A. Chaky (1993), Mineralogical variations within the S-type asteroid class, *Icarus*, *106*(2), 573–602, doi:10.1006/icar.1993.1194.
- Green, R. O., et al. (2011), The Moon Mineralogy Mapper (M^2) imaging spectrometer for lunar science: Instrument description, calibration, on-orbit measurements, science data calibration and on-orbit validation, *J. Geophys. Res.*, *116*, E00G19, doi:10.1029/2011JE003797.
- Gustafson, J. O., J. F. Bell, L. R. Gaddis, B. R. Hawke, and T. A. Giguere (2012), Characterization of previously unidentified lunar pyroclastic deposits using Lunar Reconnaissance Orbiter Camera data, *J. Geophys. Res.*, *117*, E00H25, doi:10.1029/2011JE003893.
- Hapke, B. (1981), Bidirectional reflectance spectroscopy: 1. Theory, *J. Geophys. Res.*, *86*(B4), 3039–3054, doi:10.1029/JB086iB04p03039.
- Haruyama, J., T. Matsunaga, M. Ohtake, T. Morota, C. Honda, Y. Yokota, M. Torii, Y. Ogawa, and L. W. Group (2008), Global lunar-surface mapping experiment using the Lunar Imager/Spectrometer on SELENE, *Earth Planets Space*, *60*(4), 243.
- Hawke, B. R., and J. W. Head (1980), Small dark-mantle deposits of possible pyroclastic origin: Geologic setting, composition, and relation to regional stratigraphy, in *Lunar Planet. Sci. Conf. XI*, pp. 416–417, Abstract 1148.
- Hawke, B. R., C. R. Coombs, L. R. Gaddis, P. G. Lucey, and P. D. Owensby (1989), Remote sensing and geologic studies of localized dark mantle deposits on the Moon, in *Lunar Planet. Sci. Conf. 19th*, pp. 255–268.
- Hawke, B. R., C. R. Coombs, and B. Clark (1990), Ilmenite-rich pyroclastic deposits: An ideal lunar resource, in *Lunar Planet. Sci. XX*, pp. 249–258, Lunar Planet. Inst., Houston, Tex.
- Head, J. W. (1974), Lunar dark-mantle deposits: Possible clues to the distribution of early mare deposits, in *Lunar Planet. Sci. Conf. 5th*, pp. 207–222, Pergamon Press, New York.
- Head, J. W., and L. Wilson (1979), Alphonsus-type dark-halo craters: Morphology, morphometry and eruption conditions, in *Lunar Planet. Sci. Conf. 10th*, pp. 2861–2897, Pergamon Press, New York.
- Head, J. W., and L. Wilson (1992), Lunar mare volcanism: Stratigraphy, eruption conditions, and the evolution of secondary crusts, *Geochim. Cosmochim. Acta*, *56*(6), 2155–2175, doi:10.1016/0016-7037(92)90183-J.
- Head, J. W., L. Wilson, and C. M. Pieters (2000), Pyroclastic eruptions associated with the floor-fractured lunar farside crater Oppenheimer in the South Pole Aitken basin, *Lunar Planet. Sci. XXXI*, Abstract 1280.
- Heiken, G. H., D. S. McKay, and R. W. Brown (1974), Lunar deposits of possible pyroclastic origin, *Geochim. Cosmochim. Acta*, *38*(11), 1703–1718, doi:10.1016/0016-7037(74)90187-2.
- Horgan, B. H. N., E. A. Cloutis, P. Mann, and J. F. Bell III (2014), Near-infrared spectra of ferrous mineral mixtures and methods for their identification in planetary surface spectra, *Icarus*, *234*, 132–154, doi:10.1016/j.icarus.2014.02.031.
- Isaacson, P. J., et al. (2013), Development, importance, and effect of a ground truth correction for the Moon Mineralogy Mapper reflectance data set, *J. Geophys. Res. Planets*, *118*, 369–381, doi:10.1002/jgre.20048.
- Jones, J. H., and J. W. Delano (1989), A three-component model for the bulk composition of the moon, *Geochim. Cosmochim. Acta*, *53*(2), 513–527, doi:10.1016/0016-7037(89)90402-X.
- Jozwiak, L. M., J. W. Head, M. T. Zuber, D. E. Smith, and G. A. Neumann (2012), Lunar floor-fractured craters: Classification, distribution, origin and implications for magmatism and shallow crustal structure, *J. Geophys. Res.*, *117*, E11005, doi:10.1029/2012JE004134.
- Jozwiak, L. M., J. W. Head, and L. Wilson (2015), Lunar floor-fractured craters as magmatic intrusions: Geometry, modes of emplacement, associated tectonic and volcanic features, and implications for gravity anomalies, *Icarus*, *248*, 424–447, doi:10.1016/j.icarus.2014.10.052.
- Klima, R. L., M. D. Dyar, and C. M. Pieters (2011), Near-infrared spectra of clinopyroxenes: Effects of calcium content and crystal structure: Near-infrared spectra of clinopyroxenes, *Meteorit. Planet. Sci.*, *46*(3), 379–395, doi:10.1111/j.1945-5100.2010.01158.x.
- Lucey, P. G., B. R. Hawke, C. M. Pieters, J. W. Head, and T. B. McCord (1986), A compositional study of the Aristarchus region of the moon using near-infrared reflectance spectroscopy, *Proc. Lunar Planet. Sci. 16th*, *J. Geophys. Res.*, *91*(B4), 344–354, doi:10.1029/JB091iB04p0344.
- Malaret, E., P. Guasqui, S. McLaughlin, J. Sunshine, S. Besse, R. Clark, and P. Isaacson (2011), CH1-ORB Moon M3 4 L2 reflectance near-IR spectral images V1.0, CH1-ORB-L-M3-4-L2-REFLECTANCE-V1.0, NASA Planetary Data System.
- McCord, T. B., R. N. Clark, B. R. Hawke, L. A. McFadden, P. D. Owensby, C. M. Pieters, and J. B. Adams (1981), Moon: Near-infrared spectral reflectance, a first good look, *J. Geophys. Res.*, *86*(B11), 10,883–10,892, doi:10.1029/JB086iB11p10883.
- Morris, R. V. (1976), Surface exposure indices of lunar soils—A comparative FMR study, in *Lunar Planet. Sci. Conf. VII*, pp. 315–335, Pergamon Press, New York.
- Noble, S. K., C. M. Pieters, and L. P. Keller (2007), An experimental approach to understanding the optical effects of space weathering, *Icarus*, *192*(2), 629–642, doi:10.1016/j.icarus.2007.07.021.
- Nozette, S., et al. (2010), The Lunar Reconnaissance Orbiter Miniature Radio Frequency (Mini-RF) technology demonstration, *Space Sci. Rev.*, *150*(1–4), 285–302, doi:10.1007/s11214-009-9607-5.
- Paige, D. A., et al. (2010), The Lunar Reconnaissance Orbiter Diviner Lunar Radiometer Experiment, *Space Sci. Rev.*, *150*(1–4), 125–160, doi:10.1007/s11214-009-9529-2.
- Papike, J. J., G. Ryder, and C. K. Shearer (1998), Lunar samples, *Rev. Mineral. Geochem.*, *36*(1), 5.1–5.234.
- Petro, N. E., L. R. Gaddis, and M. I. Staid (2001), Analysis of the Oppenheimer pyroclastic deposits using Clementine UVVIS data, *Lunar and Planetary Science XXXII*, Abs. 1953.
- Pieters, C., T. B. McCord, S. Zisk, and J. B. Adams (1973), Lunar black spots and nature of the Apollo 17 landing area, *J. Geophys. Res.*, *78*(26), 5867–5875, doi:10.1029/JB078i026p05867.

- Pieters, C. M., E. M. Fischer, O. Rode, and A. Basu (1993), Optical effects of space weathering: The role of the finest fraction, *J. Geophys. Res.*, 98(E11), 20,817–20,824, doi:10.1029/93JE02467.
- Pieters, C. M., L. A. Taylor, D. McKay, S. Wentworth, R. Morris, and L. Keller (2000), Spectral Characterization of Lunar Mare Soils, *Lunar Planet. Sci. XXXI*, Abstract 1865.
- Pieters, C. M., et al. (2009), The Moon Mineralogy Mapper (M3) on Chandrayaan-1, *Curr. Sci.* 00113891, 96(4), 500–505.
- Robinson, M. S., E. M. Shoemaker, and B. R. Hawke (1996), Spectral heterogeneity of lunar local dark mantle deposits, *Lunar Planet. Sci. XXVII*, pp. 1087–1088, Abstract 1544.
- Rosanova, C. E., L. Gaddis, T. M. Hare, C. Coombs, B. R. Hawke, and M. S. Robinson (1998), Characterization of “new” pyroclastic deposits on the Moon using Clementine data, *Lunar Planet. Sci. XXIX*, Abstract 1710.
- Rothery, D. A., R. J. Thomas, and L. Kerber (2014), Prolonged eruptive history of a compound volcano on Mercury: Volcanic and tectonic implications, *Earth Planet. Sci. Lett.*, 385, 59–67, doi:10.1016/j.epsl.2013.10.023.
- Schultz, P. H. (1976), Floor-fractured lunar craters, *The Moon*, 15(3–4), 241–273, doi:10.1007/BF00562240.
- Shearer, C. K., and J. J. Papike (1993), Basaltic magmatism on the Moon: A perspective from volcanic picritic glass beads, *Geochim. Cosmochim. Acta*, 57(19), 4785–4812, doi:10.1016/0016-7037(93)90200-G.
- Shearer, C. K., et al. (2006), Thermal and magmatic evolution of the Moon, *Rev. Mineral. Geochem.*, 60(1), 365–518, doi:10.2138/rmg.2006.60.4.
- Souchon, A. L., S. Besse, P. C. Pinet, S. D. Chevrel, Y. H. Daydou, J.-L. Josset, L. D’Uston, and J. Haruyama (2013), Local spectrophotometric properties of pyroclastic deposits at the Lavoisier lunar crater, *Icarus*, 225(1), 1–14, doi:10.1016/j.icarus.2013.03.004.
- Staid, M. I., et al. (2011), The mineralogy of late stage lunar volcanism as observed by the Moon Mineralogy Mapper on Chandrayaan-1, *J. Geophys. Res.*, 116, E00G10, doi:10.1029/2010JE003735.
- Sunshine, J. M., et al. (2010), Hidden in plain sight: Spinel-rich deposits on the nearside of the Moon as revealed by Moon Mineralogy Mapper (M3), *Lunar Planet. Sci. Conf. 41st*, Abstract 1508.
- Sunshine, J. M., N. E. Petro, S. Besse, and L. R. Gaddis (2014), Widespread exposures of small scale spinel-rich pyroclastic deposits in Sinus Aestuum, *Lunar Planet. Sci. Conf. 45th*, Abstract 2297.
- Tompkins, S., and C. M. Pieters (2010), Spectral characteristics of lunar impact melts and inferred mineralogy, *Meteorit. Planet. Sci.*, 45(7), 1152–1169, doi:10.1111/j.1945-5100.2010.01074.x.
- Trang, D., J. J. Gillis-Davis, J. T. S. Cahill, B. J. Thomson, R. R. Ghent, B. R. Hawke, and T. A. Giguere (2014), Physical properties of lunar localized pyroclastic deposits, *Lunar Planet. Sci. Conf. 45th*, Abstract 2307.
- Weitz, C. M., J. W. Head, and C. M. Pieters (1998), Lunar regional dark mantle deposits: Geologic, multispectral, and modeling studies, *J. Geophys. Res.*, 103(E10), 22,725–22,759, doi:10.1029/98JE02027.
- Weitz, C. M., M. J. Rutherford, J. W. Head, and D. S. McKay (1999), Ascent and eruption of a lunar high-titanium magma as inferred from the petrology of the 74001/2 drill core, *Meteorit. Planet. Sci.*, 34(4), 527–540, doi:10.1111/j.1945-5100.1999.tb01361.x.
- Wilhelms, D. E. (1968), Geologic map of the Mare Vaporum quadrangle of the Moon, Map I-548, U.S. Geol. Surv. Misc. Invest.
- Wilhelms, D. E., and J. F. McCauley (1971), Geologic map of the near side of the Moon, Map I-703, U.S. Geol. Surv. Misc. Invest.
- Wilson, L., and J. W. Head III (1981), Ascent and eruption of basaltic magma on the Earth and Moon, *J. Geophys. Res.*, 86(B4), 2971–3001, doi:10.1029/JB086iB04p02971.
- Wood, J. A., J. S. Dickey Jr., U. B. Marvin, and B. N. Powell (1970), Lunar anorthosites and a geophysical model of the moon, *Geochim. Cosmochim. Acta Suppl.*, 1, 965.
- Yamamoto, S., et al. (2013), A new type of pyroclastic deposit on the Moon containing Fe-spinel and chromite, *Geophys. Res. Lett.*, 40, 4549–4554, doi:10.1002/grl.50784.